Flow regulates biological NO3 -and N2O production in a turbid sub-tropical stream

Naomi Wells[1] and Bradley Eyre[1]

[1]Southern Cross University

November 23, 2022

Abstract

Streams play a critical role in attenuating the excess reactive nitrogen generated from human activities. These systems can consequently also emit significant amounts of N2O, a potent greenhouse gas. Models and manipulative experiments now suggest that hydrology regulates the balance between nitrogen removal and N2O production. We aimed to empirically test this hypothesis by measuring changes in the concentration and isotopic composition of NO3- (δ18O, δ15N) and N2O (δ18O, δ15N, site preference) in hyporheic sediments and surface water of a 30 m reach over eight days of falling stream discharge (2.7 to 1.8 m3 s-1). The stream was persistently heterotrophic (productivity/respiration: 0.005 - 0.2), while changes in conductivity, δ18O-H2O, and 222Rn indicated that hyporheic mixing decreased and net groundwater inputs increased as discharge declined. The shallow groundwater had high inorganic N concentrations (2 – 10 mg l-1), but increased groundwater inputs could not fully explain the concurrent increases in NO3- (1 – 3 mg N l-1) and N2O (700 to 1000 % saturation) in the surface water. Biologically, rather than solely hydrologically, regulated stream nitrogen export was confirmed by changes in N2O and NO3- isotopic composition. However, isotope patterns indicated that nitrification, not denitrification, increased surface water NO3- and N2O concentrations as hyporheic exchange decreased. These findings empirically demonstrate how flow dynamics regulate biological NO3- production as well as transport, with implications for predicting aquatic N2O emissions.

Hosted file

`essoar.10506161.1.docx` available at https://authorea.com/users/545712/articles/602125-flow-regulates-biological-no3-and-n2o-production-in-a-turbid-sub-tropical-stream

Flow regulates biological NO_3^- and N_2O production in a turbid sub-tropical stream

Naomi S. Wells[1*], Bradley Eyre[1]

[1] Centre for Coastal Biogeochemistry, School of Environment, Science & Engineering, Southern Cross University, PO Box 157, East Lismore, 2480 NSW, Australia

*Author for correspondence: naomi.wells@scu.edu.au

Under review at Geochimica et Cosmochimica Acta

Abstract

Streams play a critical role in attenuating the excess reactive nitrogen generated from human activities. These systems can consequently also emit significant amounts of N_2O, a potent greenhouse gas. Models and manipulative experiments now suggest that hydrology regulates the balance between nitrogen removal and N_2O production. We aimed to empirically test this hypothesis by measuring changes in the concentration and isotopic composition of NO_3^- ($\delta^{18}O$, $\delta^{15}N$) and N_2O ($\delta^{18}O$, $\delta^{15}N$, site preference) in hyporheic sediments and surface water of a 30 m reach over eight days of falling stream discharge (2.7 to 1.8 $m^3\ s^{-1}$). The stream was persistently heterotrophic (productivity/respiration: 0.005 - 0.2), while changes in conductivity, $\delta^{18}O$-H_2O, and ^{222}Rn indicated that hyporheic mixing decreased and net groundwater inputs increased as discharge declined. The shallow groundwater had high inorganic N concentrations (2 – 10 mg l^{-1}), but increased groundwater inputs could not fully explain the concurrent increases in NO_3^- (1 – 3 mg N l^{-1}) and N_2O (700 to 1000 % saturation) in the surface water. Biologically, rather than solely hydrologically, regulated stream nitrogen export was confirmed by changes in N_2O and NO_3^- isotopic composition. However, isotope patterns indicated that nitrification, not denitrification, increased surface water NO_3^- and N_2O concentrations as hyporheic exchange decreased. These findings empirically demonstrate how flow dynamics regulate biological NO_3^- production as well as transport, with implications for predicting aquatic N_2O emissions.

Keywords: stable isotopes, isotopomers, hyporheic zone, surface water – groundwater interactions, freshwater tidal zone, sub-tropics

1. Introduction

Excess reactive nitrogen (N) generated from human activities like agriculture and fossil fuel combustion causes a range of environmental damages, from biodiversity loss through to global climate change (Fowler et al., 2013; Galloway et al., 2008). Streams and rivers play a critical role in regulating these damages as they determine the form and quantity of N transported from land to sea (Boyer et al., 2006; McCrackin et al., 2014; Tysmans et al., 2013). However, the same conditions that maximise reactive N removal may also promote the release of nitrous oxide (N_2O), an ozone depleting greenhouse gas with 298 times the warming potential of carbon dioxide (CO_2) (Alexander et al., 2009; Quick et al., 2019; Turner et al., 2015). Evaluations of the biological and hydrological controls on reactive N removal in streams must therefore be expanded to account for potential trade-offs with N_2O emissions.

At the global scale, waterways with higher surface water nitrate (NO_3^-) concentrations tend to emit more N_2O (Hu et al., 2016; Murray et al., 2015). However, it is not yet clear whether this correlation is causal, as within-reach studies frequently show decoupling of NO_3^- and N_2O fluxes (e.g., Comer-Warner et al., 2020b). This disconnect reflects the complexity of N cycling, which can be both assimilated and/or converted via dissimilatory microbial pathways through seven redox states. Nitrous oxide is an intermediate product of both microbial N oxidation (nitrification, $NH_3 \rightarrow NO_3^-$) and reduction (denitrification, $NO_3^- \rightarrow N_2$), plus other minor microbial processes (Quick et al., 2019). Positive correlation between NO_3^- and N_2O can thus be produced by either, 1) nitrification-limited N_2O and NO_3^- production, or, 2) NO_3^--limited denitrification producing N_2O.

Stream N_2O emissions are often assumed to come primarily from denitrification (Beaulieu et al., 2011; Rosamond et al., 2012). Typically O_2 saturated surface waters confine denitrification to anoxic zones in sediments and suspended particles (Reisinger et al., 2016; Seitzinger et al., 2006; Xia et al., 2017), so stream denitrification depends on both the extent

of anoxic zone formation (capacity) and efficiency of NO_3^- transport to these anoxic zones (opportunity). Capacity is affected by C availability, sediment composition, and biological productivity (Christensen et al., 1990; Covino et al., 2018; Eyre and Ferguson, 2009; Trimmer et al., 2012). Stream hydrology controls the opportunity for N removal: slower flow velocities increase time for reactions to occur (Alexander et al., 2009; Briggs et al., 2014; Marcé et al., 2018), while vertical hyporheic zone surface water – groundwater mixing moves NO_3^- through anoxic zones (Gomez-Velez et al., 2015; Krause et al., 2017). However, N_2O fluxes are only inconsistently explained by denitrification capacity factors like NO_3^- concentrations (Hu et al., 2016), NO_3^- consumption rates (Comer-Warner et al., 2020b; Laursen and Seitzinger, 2004), or O_2 (Baulch et al., 2012; Clough et al., 2007; Reading et al., 2017; Rosamond et al., 2011; Wu et al., 2018). New models propose overcoming these inconsistencies by focusing on hydrology (opportunity). These predict that stream N_2O is highest under unstable or intermediate flow conditions, when N_2O is stripped from anoxic NO_3^- reduction zones before it can be reduced to N_2 (Marzadri et al., 2017; Quick et al., 2016). This fits with growing evidence that both opportunity and capacity must be accounted for to predict assimilatory stream N removal (Covino et al., 2018). Yet difficulty quantifying the hyporheic dynamics underpinning redox-dependent N cycling means large uncertainties persist in estimates of both stream NO_3^- removal and N_2O emissions (Hampton et al., 2020).

The aim of this study was to empirically test whether the same mechanisms control stream export of NO_3^- and N_2O. Dropping stream flow during a diurnal metabolism study provided a unique opportunity to test the hypothesis that opportunity (hydrology), more than capacity (biology), regulates stream N_2O emissions and NO_3^- removal. We measured changes in the concentration and natural abundance isotopic composition of NO_3^- and N_2O in the surface waters and porewaters (5 cm depth and 20 cm depth) of a stream both during the night v day (changing capacity) and over time as the stream height fell (changing

opportunity). This approach is based on evidence that nitrification and denitrification systematically discriminate against light isotopes (Boshers et al., 2019; Casciotti et al., 2003; Granger and Wankel, 2016) so that NO_3^- isotopic composition ($\delta^{18}O$, $\delta^{15}N$) reflects stream N cycling (Cohen et al., 2012; Wells et al., 2016). Similarly, N_2O isotopes ($\delta^{15}N$, $\delta^{18}O$) and isotopomers (intramolecular site preference of ^{15}N, SP) help constrain the relative influence of NO_3^- reduction, NH_3 oxidation, and N_2O reduction on N_2O fluxes (Ostrom and Ostrom, 2017; Well et al., 2012).

2. Materials & Methods

2.1 Site description

The study was carried out in Monaltrie / Gundurimba Creek, which drains into the Wilson River in Lismore, New South Wales, Australia (28°50'57"S, 153°16'27"E) (Fig. 1). The stream is tidal with muddy sediments. The site is underlain by fractured basalt, including unconfined shallow aquifers, and sharp topography constrains water flow paths (Brodie et al., 2007; Brodie et al., 2003). The region has a semi-tropical climate with warm, wet summers and cool, dry winters, with mean temperatures ranging from 13°C to 28°C. Mean annual rainfall is 1,200 mm rain. Effluent from a nearby wastewater treatment plant (WWTP) discharges into Monaltrie Creek and the shallow groundwater upstream from the study site (Fig. 1), leading to elevated DIN concentrations in both the surface and groundwater (Table 1). Local shallow groundwater is ~21°C and the surface water between 19 and 27 °C.

2.2 Experimental design

Surface water (*SW*), surface sediment porewaters (*S*), and hyporheic zone water (*HZ*) were sampled at nine locations across a 30 m stream reach over five 24 h periods spanning eight days in April 2017 (late summer). We logged changes in N_2O, as well as supporting

chemical (O_2, CO_2, CH_4, conductivity) and hydrologic (radon, ^{222}Rn, as a proxy for groundwater inputs, as well as temperature, flow velocity, and stream height) parameters every 1 s^{-1} – 30 min^{-1} in the centre of the sampled reach. This intensive local sampling design enabled us to identify 'hot spot' zones of surface water -groundwater interactions and directly relate subsurface processes to temporal surface dynamics. Discrete samplings were timed to the O_2 maxima and minima of each day in order to fully capture stream N variability (Baulch et al., 2012; Christensen et al., 1990): samples were collected at 02:00 and 14:00 on D1, D2, and D4, then at low and high tides for D6 and D8 after reviewing O_2 data. Climate data (wind speed, air temperature, rainfall) was downloaded from the Bureau of Meteorology station (http://www.bom.gov.au/climate/dwo/IDCJDW2074.latest.shtml, accessed 16/06/2017).

2.2.1 Discrete samples

Surface water samples were collected by filling a 1 L bottle and then sub-sampling into vials using a 20 ml syringe (Fig. 1). For the surface sediments (*S*), diffusive equilibration in thin-film (DET) probes were degassed for 8 hr in a 0.01M NaCl solution purged with N_2, then installed to 5 cm depth six hours prior to sampling (Huang et al., 2016; Huang et al., 2019). Probes were collected prior to the surface grab samples and stored wrapped in cellophane. Hyporheic samples were collected from piezometers (20 cm internal diameter) installed 20 cm below the sediment surface. A 50 ml syringe was used to collect *HZ* water, with the first 50 ml discarded to purge the well. The *SW* and *HZ* samples were either passed through 0.22 µm syringe tip filters (polyethersulfone, Minisart) for inorganic nutrient (PO_4^{3-}, NO_3^-, and NH_4^+) and NO_3^- dual isotope analyses, or passed through a 0.45 µm syringe tip filter (polyethersulfone, Minisart) into a pre-combusted 40 ml glass vial sealed with a Teflon septa for organic carbon (DOC) analysis. Samples were frozen at -20°C until analysis. Additional surface water samples for $\delta^{15}N\text{-}N_2O$, $\delta^{18}O\text{-}N_2O$, and $SP\text{-}N_2O$ were collected in

500 ml glass crimp-top bottles (Wheaton). These were stored in the dark at 4°C, and analysed within one month of collection. Conductivity (Eutech Instruments) in *HZ* and *SW* samples, and temperature and O_2 (Hach LDO) in *HZ* samples, were measured in the field prior to filtering. The DET probes were cut along the sediment – surface water line, placed into a sterile plastic vial, and frozen at -20°C until analysis.

2.2.2 Continuous measurements

Loggers were installed at B2 (Fig. 1). Flow velocity (*v*) and water depth (*h*) were logged every 10 min using an ultrasonic Doppler instrument (Starflow, Unidata) placed on the sediment surface, and water chemistry, including DO, logged every 30 minutes using a Hydrolab HL4 installed 20 cm below the water surface. Other dissolved gasses (^{222}Rn, CO_2, CH_4, and N_2O) were measured by continuously pumping water from 20 cm below the surface through a showerhead exchanger (Durridge). Air from the exchanger was pumped through a Drierite column to remove moisture, and then to either a Picarro G2308 (N_2O, CH_4), LI-COR LI-820 (CO_2), or a Durridge RAD7 (^{222}Rn). Carbon dioxide and N_2O concentrations were logged ~1 s^{-1} and ^{222}Rn every 10 min. Measurement precision was 0.05% for N_2O. Picarro stability was confirmed prior to use using N_2 (0 ppm N_2O) and N_2O (28 ppm) gasses. The LI-COR was calibrated prior to deployment (0 ppm, 1000 ppm), and had 1 ppm precision.

2.3 Sample analyses

Inorganic nutrient concentrations were measured using a Lachat Flow Injection Analyser, see Eyre and Pont (2003) for details. Note NO_3^- was measured as NO_3^-+NO_2^- and NH_4^+ as NH_3+NH_4^+. DOC concentrations were measured via continuous flow wet oxidation on an Aurora 1030W TOC analyser. For *S* samples, DET gels were extracted overnight using

10 ml deionised water, which was then analysed for NO_3^- and NH_4^+ concentrations and NO_3^- dual isotope composition (Comer-Warner et al., 2017; Huang et al., 2016).

Water isotopes ($\delta^{18}O$-H_2O) in *SW* and *HZ* samples was measured on a High Temperature Conversion Elemental Analyzer (Thermo-Fisher TC-EA) coupled to an IRMS (Thermo-Fisher Delta-V plus) via a Thermo-Fisher ConFlo IV. Samples were measured 5x (1 µL injection) to account for carryover, and calibrated using VSMOW2 ($\delta^{18}O$ = 0.0‰) and SLAP2 ($\delta^{18}O$ = -55.5‰) standards. Dual NO_3^- + NO_2^- isotopes ($\delta^{15}N$ and $\delta^{18}O$) were measured using a *Pseudomonas aureofaciens* culture genetically modified to block N_2O reduction to quantitatively convert NO_x^- to N_2O (McIlvin and Casciotti, 2011). Sample batches were prepared along with triplicate culture blanks and the internationally certified standards USGS34, USGS32, and USGS35. The produced $\delta^{15}N$ and $\delta^{18}O$ composition of the produced N_2O was measured using a Thermo Fisher Delta V Plus IRMS fitted with a custom gas bench (Thermo Fisher Gasbench II). The isotopic composition of *SW* N_2O ($\delta^{15}N$-N_2O, $\delta^{18}O$-N_2O, and SP, where SP = $^{\alpha}N$ - $^{\beta}N$) was measured after injecting a 50 ml helium headspace into the 500 ml sample bottles, allowing samples to equilibrate for >2 hr, and adjusting the gas bench for manual injection (Murray et al., 2018). Data were corrected offline as described in Toyoda and Yoshida (1999), and calibrated from triplicate measurements of three internationally-verified N_2O isotope standards (Mohn et al., 2014).

2.4 Data analysis

Analyses were carried out in R v 4.0 / R Studio v 1.3.959. Stream discharge (Q, m^3 s^{-1}) was calculated from the logged flow velocity (v, in m s^{-1}) and reach cross-sectional area (width × h). Downstream discharge of DOC and NO_3^- was calculated as the measured concentration (g m^{-3}) × Q (m^3 s^{-1}) for the 3 h around sample collection. Water chemistry differences were determined using mixed models, with sample locations as repeated

measures, time and depth as continuous variables, and width and length locations as fixed factors, using lmer4 and merTools (Bates et al., 2015; Knowles and Frederick, 2019). Due to sample numbers, tests were run separately for each depth layer. Figures were generated with ggplot2, patchwork, and ggpubr (Kassambara, 2020; Pedersen, 2019; Wickham, 2016).

2.4.1 Biogenic gasses

Gross primary productivity (GPP) and ecosystem respiration (ER) were estimated as functions of light using a maximum likelihood estimation model from streamMetabolizer R (Appling et al., 2018). Estimates were based on measured O_2 concentrations, water temperatures, Q, h, and the estimated solar radiation for the location × time.

N_2O, CO_2, and CH_4 data were block-averaged at 1 min^{-1} intervals, and dissolved concentrations calculated based on the partial pressure (µatm) and solubility (K_0, in mol atm^{-1} l^{-1}) calculated for each gas for a given temperature and conductivity. Dissolved ^{222}Rn concentrations (dpm l^{-1}) were calculated as per Santos et al. (2012), dissolved N_2O (µg N l^{-1}) using the K_0 defined in Weiss and Price (1980), and CO_2 (mg l^{-1}) as per Wanninkhof (2014). Time-lags created by variable gas equilibration times were applied to the data using values previously calculated for this sampling set-up (15 min for N_2O and CO_2, 30 min for ^{222}Rn) (Erler et al., 2015; Maher et al., 2013; Santos et al., 2012). The transfer velocity between the surface water and air (k), which is regulated by v and h (Hall and Ulseth, 2019), was calculated for each 1 min of data using three of the empirical equations outlined in (Raymond et al., 2012) and used to calculate mean daily water-to-air N_2O fluxes (Suppl. Mat. 1).

Dissolved N_2O isotope and isotopomer values were corrected for mixing with atmospheric N_2O to ensure that variations in concentrations did not bias the data, as suggested by (Thuss et al., 2014). This was done using a two-pool mixing model (Eq. 1):

(Eq. 1) $$\delta_{measured} = f_{air}\delta_{air} + f_{stream}\delta_{stream}$$

$$1 = f_{air} + f_{stream}$$

where f_{air} is defined based on N_2O saturation, making this a conservative estimate of two-way air-water mixing (Eq. 2):

$$f_{air} = \frac{0.32 \times K_0}{N2O_{measured}} \quad \text{(Eq. 2)}$$

where 0.32 is the partial pressure of N_2O in the air and $N_2O_{measured}$ is the measured partial pressure dissolved in the surface water. We then solved Eq. 1 assuming that 'air' N_2O had the concentration and isotopic composition of tropospheric N_2O: $\delta^{15}N\text{-}N_2O$ = 7.0 ‰, $\delta^{18}O\text{-}N_2O$ = 43.7 ‰, SP = 18.7 ‰ (Yoshida and Toyoda, 2000). Dissolved $\delta^{18}O\text{-}N_2O$ values were normalised to surface water $\delta^{18}O\text{-}H_2O$ values (Lewicka-Szczebak et al., 2017), to correct for O exchange during N_2O production (Snider et al., 2009; Snider et al., 2013).

2.4.2 Surface water – groundwater interactions

Two approaches helped constrain surface water – groundwater mixing. First, the proportion of surface water in the hyporheic zone was estimated from conductivity (Eq. 3):

$$f_{sw} = \frac{C_{GW} - C_{HZ}}{C_{GW} - C_{SW}} \quad \text{(Eq. 3):}$$

where conductivity measured in sub-surface wells (C_{HZ}) is compared to the range of conductivity range reported for shallow site groundwater (C_{GW}; Table 1) and measured in the surface water (C_{SW}). Eq. 3 was solved for each sampling point using the mean ± SD of each parameter. Second, the measured diurnal ^{222}Rn fluctuations were used to approximate groundwater inputs to the surface water. This approach is based on the knowledge that relatively short surface water ^{222}Rn residence times mean that measured concentrations must come from subsurface inputs (Burnett et al., 2010; Khadka et al., 2017). The groundwater flux into the surface water (Q_{GW}, in $m^3\ s^{-1}$) was estimated by mass balance (Eq. 4):

$$Q_{GW} = \frac{F_{decay} + F_{air} + Q_{low}Rn_{low} - Q_{high}Rn_{high}}{Rn_{GW}} \quad \text{(Eq. 4):}$$

where F_{decay} is ^{222}Rn removal due to radioactive decay and F_{air} is the ^{222}Rn water-air flux, calculated using constants and parameterisations from Burnett et al. (2010), and the measured differences between ^{222}Rn fluxes at low ($Q_{low} \times Rn_{low}$, in $m^3\ s^{-1} \times dpm\ m^{-3}$) and high ($Q_{high} \times Rn_{high}$) tides approximate upstream ^{222}Rn inputs v. downstream exports, respectively. This defines Q_{GW} as the ^{222}Rn flux not explained by hydrology. Eq. 4 was solved for each 24 h sampling period using the maximum and minimum ^{222}Rn concentrations (230,000 dpm m^{-3} and 20,000 dpm m^{-3} for local shallow groundwater (Atkins et al., 2013; Gatland et al., 2014). Note that end-member uncertainty means that Eq. 3 and Eq. 4 help constrain, but do not precisely quantify, changes in surface water – groundwater interactions over time.

3. Results

3.1 Hydrology

Stream height fluctuated tidally by ~0.1 m. Daily *v* peaks (up to ~2 m s^{-1}) coincided dips in *h* minima (Fig. 2) and conductivity (r = 0.4 – 0.7, p<0.001). Surface water was 21 ± 0.5 °C. Over time k_{600} values ranged from 1.3 ± 0.3 m d^{-1} to 0.73 ± 0.3 m d^{-1} (Suppl. Mat. Table S1). Over time *h* declined from 1.1 to 0.86 m (p<0.001), *Q* decreased from 3 $m^3\ s^{-1}$ to ~2 $m^3\ s^{-1}$ (p<0.001), and conductivity increased (p<0.001; Suppl. Mat. Table S3). Surface water $\delta^{18}O\text{-}H_2O$ decreased over time (F = 17, p<0.001) (Table 2, Fig. 2). The ^{222}Rn × conductivity relationship differed between days (F = 83, p<0.001), with the slope becoming more negative from D1 (x = -0.008, p<0.001, r^2 = 0.19) to D6 (x = -0.07, p<0.001, r^2 = 0.34), and the estimated marginal mean increased from 3.7 dpm l^{-1} (D1, D2) to 4.1 dpm l^{-1} (Fig. 2). Solving Eq. 4 for the daily ^{222}Rn and *Q* fluctuations indicated that groundwater contributions to surface water increased from 35 ± 30 % on D1 to 61 ± 50 % on D8 (Table 3).

Temperature in *HZ* (22°C) did not differ significantly from *SW*, nor between night and day (Table 1). The $\delta^{18}O\text{-}H_2O$ values differed between surface and subsurface waters (F =

4, $p<0.05$). Subsurface $\delta^{18}O\text{-}H_2O$ values decreased over time (F = 3.3, $p<0.01$), particularly along the north bank, where values tended to be most negative (location: F = 7.8, $p<0.05$; date × location: F = 3.4, $p = 0.06$) (Table 2). Conductivity was greater in *HZ* than *SW* (F = 300, $p<0.001$; Table 2). *HZ* conductivity increased over time (680 ± 50 µS cm^{-1} to 1,200 µS cm^{-1}; F = 160, $p<0.001$), particularly along the north bank (F = 9.3, $p<0.05$; date × location: F = 30, $p<0.001$). Mass balances based on *HZ* and *SW* conductivity (Eq. 3) show surface water contributions to the subsurface decreased from 83 % on D1 to 62 % on D8 (Table 3).

3.2 Biogenic gasses (O_2, CO_2, N_2O)

Surface water O_2 concentrations varied diurnally from 1.6 ± 0.2 mg l^{-1} (20% saturation) to 1.4 ± 0.2 mg l^{-1} (15% saturation) ($p<0.001$), and decreased from 1.5 ± 0.4 on D1 to 1.4 ± 0.1 mg O_2 l^{-1} on D8 ($p<0.001$; Fig. 2). Best-fit metabolism models accounted for between 60% (D4) and 90% (D6) of diurnal O_2 fluctuations (Suppl. Mat. Fig. S1). Model estimated GPP was 1.3 (0.7 – 3) g O_2 m^{-2} d^{-1} and ER was -28 (-60 - -3) g O_2 m^{-2} d^{-1}, producing a GPP/ER ratio of 0.08 (0.03 – 0.1) over the study period (Table 3).

Daily dissolved CO_2 negatively correlated with O_2 fluctuations (r = -0.36, $p<0.001$; Fig. 2). Over time CO_2 increased from 3.1 ± 0.06 mg C l^{-1} to 3.2 ± 0.03 mg C l^{-1} ($p<0.001$; Fig. 2) and the CH_4:CO_2 concentration ratio decreased from 0.013 to 0.0088 ($p<0.001$; Suppl. Mat Fig. S2). Daily N_2O fluctuations negatively correlated with h (r = -0.79, $p<0.001$), ^{222}Rn (r = -0.067, $p<0.05$), and O_2 (r = -0.39, $p<0.001$), and positively correlated with conductivity (r = 0.89, $p<0.001$). Concentrations increased over time from 1.4 µg N_2O-N l^{-1} on D1 to 2.6 µg N_2O-N l^{-1} on D8 ($p<0.001$; Fig. 2), as did estimated marginal means relative to conductivity (690 ± 2 % saturation on D2, 930 ± 3 % saturation on D8). The relationship between N_2O and O_2 saturations changed over time (F = 280, $p<0.001$) from negative on D1 and D2 (r = -0.6) to positive on D4 – D8 (r = 0.1).

299

300 3.3 Stream nutrients

301 Nutrient (DOC, PO_4^{3-}, NO_3^-, NH_4^+) concentrations did not differ significantly
302 between 'low O_2' and 'high O_2' sampling points in either the *SW*, *S*, or *HZ* samples. Data are
303 therefore presented as the daily mean for each 24 h period. Surface waters NO_3^-
304 concentrations increased over time (Suppl. Mat. Table S8), while DOC, and NH_4^+
305 concentrations decreased (Table 2). Nitrate was 50% of *SW* inorganic N on D1 v. 80% on D8.
306 Nitrate concentrations tended to be highest along the south bank, both in absolute terms and
307 relative to conductivity (Table 2). Ammonium tended to be highest along the north bank and
308 towards the top of the reach (Fig. 3). Nitrate was always higher in *SW* than

309 Surface sediment (*S*) NO_3^- concentrations decreased from 0.62 mg N l^{-1} on D1 to 0.39
310 mg N l^{-1} on D8 ($F = 6.6$, $p<0.05$), while *S* NH_4^+ concentrations remained relatively consistent
311 over time (Fig. 3; Suppl. Mat. Table S8). This zone had the highest NH_4^+ concentrations (*S* >
312 *HZ* > *SW*) and lowest NO_3^- concentrations (*S* < *HZ* < *SW*) (Fig. 3). Spatially, *S* NH_4^+ was
313 highest in the centre, while NO_3^- increased from the north bank (0.34 ± 0.3 mg N l^{-1}) to centre
314 (0.39 ± 0.3 mg N l^{-1}) to south bank (0.57 ± 0.4 mg N l^{-1}) ($F = 4.0$, $p<0.05$; Fig. 3).

315 Deeper sediment (*HZ*) NO_3^- concentrations increased over time along the south bank
316 and downstream, while NH_4^+ increased upstream along the north bank (Fig. 3). Over time
317 NO_3^-:conductivity ratios and DOC concentrations increased at all *HZ* sites (Table 2).
318 Ammonium concentrations were highest along the north bank (2.3 ± 2 mg N l^{-1}), where NO_3^-
319 concentrations were lowest (0.12 ± 0.2 mg N l^{-1}). The *HZ* NO_3^- concentrations were lower
320 upstream (0.48 ± 0.5 mg N l^{-1}) than downstream (1.1 ± 0.8 mg N l^{-1}) ($p<0.01$, Fig. 3), while
321 DOC concentrations were highest along the north bank (Table 2).

322

323 3.4. Isotopic composition of inorganic N species

3.4.1 Nitrate ($\delta^{18}O$, $\delta^{15}N$)

Nitrate isotopes did not differ significantly night v day / high v low tide in either *SW*, *S*, or *HZ*, so data is presented as the mean for each 24 h period. The $\delta^{15}N\text{-}NO_3^-$ and $\delta^{18}O\text{-}NO_3^-$ values varied significantly over the reach width in *S* and *HZ* (not SW), but did not vary over reach length at any depth (Suppl. Mat. Table S8). $\delta^{15}N\text{-}NO_3^-$ and $\delta^{18}O\text{-}NO_3^-$ had distinct patterns over time (Fig. 4). On D1 near-bank $\delta^{15}N\text{-}NO_3^-$ was +7 ‰ higher in *HZ* than *S*, but this reversed on D4 – D8 with values 0.6 ‰ higher in *S* than *HZ* (Fig. 4). In contrast, *S* $\delta^{18}O\text{-}NO_3^-$ values were consistently higher than both *SW* and *HZ* (Fig. 4). Over time *S* $\delta^{18}O\text{-}NO_3^-$ increased, especially along the north bank ($F = 8.6$, $p<0.01$), so the difference between *S* and *SW* $\delta^{18}O\text{-}NO_3^-$ went from 9.8 ‰ (D1, D2) to 11 ‰ (D6, D8) (Fig. 5).

Surface water NO_3^- concentrations correlated with $\delta^{15}N\text{-}NO_3$- ($r = 0.63$, $p<0.001$), but not $\delta^{18}O\text{-}NO_3^-$. Over time *SW* $\delta^{15}N\text{-}NO_3^-$ increased (12 ± 0.5 ‰ to 13 ± 0.2 ‰) while $\delta^{18}O\text{-}NO_3^-$ decreased (3.9 ± 3 ‰ to 0.35 ± 2 ‰) (Fig. 4). Surface sediment $\delta^{18}O\text{-}NO_3^-$ values were highest along the north bank (13 ± 4 ‰) and $\delta^{15}N\text{-}NO_3^-$ values highest in the centre (16 ± 7 ‰). Over time south bank *S* $\delta^{15}N\text{-}NO_3^-$ increased (7.7 ± 2 ‰ to 20 ± 6 ‰) and $\delta^{18}O\text{-}NO_3^-$ decreased (16 ± 5 ‰ to 10 ± 2 ‰; Fig. 4). In *HZ* the $\delta^{18}O\text{-}NO_3^-$, but not $\delta^{15}N\text{-}NO_3^-$, decreased from the north bank (9.2 ± 6 ‰) to centre (4.9 ± 6 ‰) to south bank (4.0 ± 2 ‰). Over time *HZ* $\delta^{15}N\text{-}NO_3^-$ decreased from 15 ± 10 ‰ on D1 to 13 ± 1 ‰ on D6 (Fig. 5). Accordingly, the linear relationship between $\delta^{18}O\text{-}NO_3^-$ v $\delta^{15}N\text{-}NO_3^-$ was never strong, but shifted from weakly negative in *SW* (slope = -0.7, $p<0.001$, $r^2 = 0.04$) to more clearly negative in *S* (slope = -0.3, $p<0.001$, $r^2 = 0.14$), to positive in *HZ* (slope = 0.5, $p<0.001$, $r^2 = 0.19$).

3.4.2 N_2O ($\delta^{18}O$, $\delta^{15}N$, SP)

Nitrous oxide isotopes ($\delta^{18}O$, $\delta^{15}N$, and SP), measured at the nine *SW* sampling locations, differed neither between day/night samplings nor between locations (Suppl. Mat.

Fig. S3). Over time $\delta^{15}N\text{-}N_2O$ values decreased from 1.5 ± 2 ‰ to -0.99 ± 0.9 ‰ ($F = 26$, $p<0.001$; Fig. 6). The $\delta^{18}O\text{-}N_2O$ values were lower on D1 (52 ± 6 ‰) than D2 – D8 (57 ± 4 ‰) ($F = 20$, $p<0.001$), while SP increased from 15‰ on D1 to 31‰ on D8 ($F = 200$, $p<0.001$). Changes in $\delta^{18}O\text{-}N_2O$ related inversely to $\delta^{15}N\text{-}N_2O$ ($y = 16 – 0.26x$, $p<0.001$, $r^2 = 0.45$) and positively to SP ($y = -56 + 1.3x$, $p<0.001$, $r^2 = 0.61$) (Fig. 6). Consequently, the difference between $\delta^{18}O\text{-}N_2O$ and $\delta^{18}O\text{-}NO_3^-$ at each site increased over time from 49‰ to 58‰ ($F = 15$, $p<0.001$), while $\delta^{15}N\text{-}N_2O$ decreased relative to the corresponding $\delta^{15}N\text{-}NO_3^-$ from -10‰ on D1 to -14‰ on D8 ($F = 90$, $p<0.001$).

4. Discussion

4.1 Hydrologic setting

Tides often dominant daily water chemistry fluctuations at the marine end of estuaries (Call et al., 2015), but were expected to be secondary to internal productivity in this nutrient-rich freshwater zone ~100 km inland (Knights et al., 2017). The distinctly tidal fluctuations in depth, *v* and conductivity (Fig. 2) are likely made more apparent due turbidity masking any diurnal metabolism. The fact that daily ^{222}Rn fluctuated with *v* and *h* also suggests the tidal shifts in hydraulic pressure could be 'pumping' the subsurface and influence hyporheic exchange (Barnes et al., 2019; Bianchin et al., 2011). However, these daily fluctuations are overprinted by continuous declines in *h* and *Q* (Fig. 2, Table 2). Decreasing *Q*, which could promote internal N reactions over downstream discharge (Ocampo et al., 2006; Raymond et al., 2016; Wollheim et al., 2018), is clear. Yet the *h* and *v* shifts could also alter microbial N transformations vis-à-vis subsurface exchange (Hester et al., 2019; Krause et al., 2017; Lewandowski et al., 2019; Singh et al., 2019).

Multiple lines of evidence suggest that the connection between surface water and groundwater changed over the study period. The increased surface water ^{222}Rn (Table 3) fits

expectations that groundwater inputs decrease during high flow events and then increase as the system returns to baseflow (Looman et al., 2016; Schubert and Paschke, 2015; Webb et al., 2017). However, this is complicated by the concurrent dampening tidal ^{222}Rn fluctuations, which suggest weakening tide-driven pumping, and thus vertical mixing (Call et al., 2015). Decreased vertical mixing during the return to baseflow conditions is supported by, first, the growing spatial variability in subsurface $\delta^{18}O\text{-}H_2O$, as incomplete mixing is needed for isotopically distinct pools to develop (Dudley-Southern and Binley, 2015), and, second, increased difference between surface and subsurface conductivities (Table 3). Thus falling *v* and *h* led to both more groundwater dominated surface waters and dampened vertical exchange within the channel. This provides a strong framework for empirically evaluating hydrologic regulations of stream NO_3^- and N_2O processing.

4.2 Biological setting (metabolism)

Diurnal light variations that shift streams from net respiration (O_2 consuming) at night to net photosynthesis (O_2 producing) during the day (Bernhardt et al., 2018; Parker et al., 2005) can impact N cycling (Martí et al., 2020; Yang et al., 2019). Previous work shows that NO_3^- concentrations similar to those measured here can fuel biological growth to the extent that O_2 fluctuates >100% between night and day (Clough et al., 2007; Harrison et al., 2005). Yet despite the warm temperatures and high nutrient concentrations, daily O_2 varied by only 5% (Fig. 2). Notably, unlike other systems where muted diurnal O_2 signals reflected low biological activity (e.g., Baulch et al., 2012), here the low O_2 (~ 20% saturation) and high CH_4:CO_2 ratios instead indicate strong heterotrophy (Stanley et al., 2016). This fits with metabolism model estimates that reach respiration was 5 – 20 times higher than productivity (Table 3). A strongly heterotrophic system is reasonable given the observed low water clarity that would inhibit photoautotrophic activity (see photos in Fig. 1, Fig. 7) and high nutrient

loads to fuel respiration. This contradicts the expectation that increased nutrients + light fuel plant growth in highly impacted waterways (Tank et al., 2010). However, we observed a similar turbidity-driven productivity drop in other highly modified subtropical waterways (Wells and Eyre, 2019; Wells et al., 2020). The markedly low productivity here thus provides a critical contrast to previous metabolism × N investigations, which found light fluctuations drove N uptake vis-à-vis primary productivity (Fork and Heffernan, 2014; Hall and Tank, 2003; Reisinger et al., 2019). For our purposes the key implications of the apparently light-limited metabolic regimen are that, 1) assimilatory phototrophic N demand will be minimal, and, 2) low O_2 and high C create favourable denitrification conditions.

4.3 Nitrate

The increasing surface water NO_3^- concentrations over time contradict the hypothesis that *Q* regulates solute export by decreasing in-stream processing (Alexander et al., 2009; Raymond et al., 2016; Wollheim et al., 2018). Downstream NO_3^- export actually increased from 250 to 410 kg N d^{-1} despite *Q* decreasing by 30% (Fig. 7). Similar NO_3^- increases following hydrologic 'pulses' were previously observed (Chen et al., 2020; McKee et al., 2000; Ocampo et al., 2006), but it is unclear whether this is due to either new NO_3^- sources entering the system or changing internal N cycling.

4.3.1. Hydrologic NO_3^- sources

Increased solute export following high-flow events can come from either overland flow or increased groundwater inputs (Ocampo et al., 2006; Webb et al., 2017). A new upstream source emerging during this study's narrow sampling window can be reasonably ruled out due to the magnitude of the established WWTP source and lack of branching tributaries (Fig. 1). However, infiltration of shallow, N-rich groundwater (Table 1) could

affect surface water NO_3^-. Significant groundwater NO_3^- inputs aligns with evidence that groundwaters comprised a greater proportion of stream flow over time (Table 3), and is supported by the spatial distribution of streambed N. The highest sediment N concentrations cluster along the north bank near the groundwater plume (Fig. 1, Fig. 3) and NO_3^- depth profiles are inverted relative to what is created when surface water is the sole NO_3^- source (Kessler et al., 2013; Schutte et al., 2015). However, the significance of groundwater N to the measured surface water concentrations would depend on the extent of denitrification during transport through the sediments (Trauth and Fleckenstein, 2017; Trauth et al., 2014). Changes in NO_3^- isotopic composition constrain this factor: conservative groundwater-to-surface water transport (no sediment denitrification) would cause *SW* NO_3^- to become isotopically similar *HZ* NO_3^- as the groundwater contribution increased, while reactive transport (incomplete sediment denitrification) would fractionate upwelling NO_3^- and cause *SW* NO_3^- to become isotopically heavier than *HZ* NO_3^- (Wells et al., 2019). Neither scenario is reflected in the relatively low *SW* δ^{15}N-NO_3^- and δ^{18}O-NO_3^- values that persisted throughout the study (Fig. 5). Instead, the increasing isotopic depletion, rather than enrichment or equivalence, of *SW* NO_3^- relative to subsurface NO_3^- shows that the net increase in upwelling groundwater was not the main driver of increasing surface water NO_3^-. This indicates that changing within-stream cycling, rather than external inputs, regulated NO_3^- concentrations.

4.3.2. Biological NO_3^- cycling

Relatively warm water temperatures and high substrate concentrations would provide ample 'capacity' for a range of N transformations within the sampled reach. However, the apparently light-limited stream productivity also negated the photoautotrophic nutrient demand, which would cause diel surface water NO_3^- concentration fluctuations (Appling and Heffernan, 2014; Chamberlin et al., 2019; Cohen et al., 2012). This finding is important as it

449 suggests that dissimilatory microbial pathways, rather than assimilation and mineralisation by
450 algae and plants, are the likely drivers of stream N dynamics.

451 Increasing surface water NO_3^- export could come from either decreased removal
452 (denitrification) or increased production (nitrification). The changed flow dynamics and
453 hyporheic exchange would affect the opportunity for both to occur (Azizian et al., 2017;
454 Briggs et al., 2014; Harvey et al., 2013; Naranjo et al., 2015). Denitrification can be limited
455 under high flows when there is insufficient time for anoxic zones to form (Kessler et al.,
456 2013; Zarnetske et al., 2012). Nitrification is maximised under 'intermediate' flows that limit
457 the extent of anoxic sites (Azizian et al., 2017; Zarnetske et al., 2012). Declining hyporheic
458 exchange, which regulates stream denitrification by transporting NO_3^- to denitrifying zones
459 (Gomez-Velez et al., 2015), could also shift the nitrification-denitrification balance.

460 Nitrate isotopes help tease apart the relative importance of decreasing denitrification v
461 increasing nitrification on surface water NO_3^- fluxes. First, denitrification causes a
462 characteristic parallel enrichment in $\delta^{15}N\text{-}NO_3^-$ v $\delta^{18}O\text{-}NO_3^-$ (Granger and Wankel, 2016;
463 Wells et al., 2019), which was not evident here (Fig. 4). Second, nitrification can be
464 constrained based on $\delta^{18}O\text{-}NO_3^-$ values because nitrifiers incorporate O from the surrounding
465 water and dissolved O_2. Assuming these are incorporated at a ratio of $2\times O\text{-}H_2O$ to 1 x $O\text{-}O_2$
466 (Kendall, 1998), and using measured $\delta^{18}O\text{-}H_2O$ values and 23.5‰ for $\delta^{18}O\text{-}O_2$ (Kroopnick
467 and Craig, 1972), here nitrification-produced $\delta^{18}O\text{-}NO_3^-$ values would be ~5‰ (Fig. 5).
468 However, this common parameterisation likely over-estimates $\delta^{18}O\text{-}NO_3^-$ as it does not
469 account for fractionation during incorporation or exchange with surrounding H_2O (Buchwald
470 et al., 2012). Thus any within-stream nitrification here likely produced $\delta^{18}O\text{-}NO_3^-$ values
471 between -10‰ (Fang et al., 2012) and -4‰ (Boshers et al., 2019). Although admittedly
472 broad, surface water $\delta^{18}O\text{-}NO_3^-$ clearly shifted to this 'nitrification' range over time while

sediment $\delta^{18}O\text{-}NO_3^-$ values remained relatively enriched (Fig. 5). In-situ production, rather than decreased removal, thus likely increased surface water NO_3^- export over time.

Increasing nitrification as hyporheic exchange declined is reasonable in this setting. First, the low light conditions would favour nitrification. Aquatic nitrification is generally highest when turbidity or depth inhibit phytoplankton growth, removing competition for any available NH_4^+ (Smith et al., 2014; Stephens et al., 2019; Xu et al., 2019). Second, stream sediments would provide an ample NH_4^+ supply to the overlying water (Fig. 3), regardless of the potential ~10% bias associated with the *S* DET probes (Briggs et al., 2015; Comer-Warner et al., 2020a). While very high, the porewater concentrations fit within the ~30 – 100 mg NH_4^+-N l^{-1} range of other sewage-impacted (Gupta and Karuppiah, 1996; Palmer-Felgate et al., 2010) and hypereutrophic (Morgan et al., 2012) systems. We therefore proposed that decreased hyporheic mixing increased NO_3^- release into the surface water (net nitrification) by minimising transport between oxic (NO_3^- rich) and anoxic (denitrifying) microsites in the subsurface (Harvey et al., 2013; Kessler et al., 2013).

4.4 Surface water N_2O cycling

Increasing N_2O emissions could result from decreased reduction or increased production via either denitrifying or nitrifying pathways. However, like NO_3^- export, stream N_2O emissions are often assumed to be regulated by denitrification (Beaulieu et al., 2011; Hampton et al., 2020). This is partially based on inverse O_2:N_2O relationships observed between days, seasons, and systems (Ji et al., 2018; Laursen and Seitzinger, 2004; Rosamond et al., 2012; Venkiteswaran et al., 2014). Here a similar negative O_2:N_2O relationship was found on the first two sampling dates (Fig. 2). This relationship could reflect stream biology, with sediment oxygenation at high tide inhibiting denitrification (Barnes et al., 2019; Knights et al., 2017)). Alternatively, tidal flushing of N_2O rich, O_2 poor porewaters at low tide would

produce the same pattern (Reading et al., 2017). It then follows that the shift towards a positive O_2:N_2O relationship that emerged on the subsequent three sampling dates (Fig. 2) was due to either a shift away from denitrification-driven (O_2-limited) N_2O production or tidal flushing decreasing along with hyporheic exchange.

The N_2O isotope data confirmed that in-stream biological production changed over time as N_2O emissions increased (Fig. 6, Fig. 7). Increasingly negative $\delta^{15}N$-N_2O values over time could be caused by either increasing nitrification (^{15}N enrichment factor, $^{15}\varepsilon$, of -56‰ for $NH_2OH \rightarrow N_2O$) relative to bacterial denitrification ($^{15}\varepsilon$ = -20‰ for $NO_2^- \rightarrow N_2O$) or a decline in N_2O reduction to N_2, which progressively enriches the residual N_2O pool ($^{15}\varepsilon$ = -6 – 7 ‰) (Denk et al., 2017; Lewicka-Szczebak et al., 2017). Yet here the simultaneous increases in SP and $\delta^{18}O$-N_2O clearly confirm that increased N_2O over time was produced by net nitrification increasing, not denitrification or N_2O reduction (Fig. 5). This is because, 1) nitrification produces N_2O with higher SP (~30, (Frame and Casciotti, 2010)) than microbial denitrification (SP ~0, (Haslun et al., 2018)), 2) the SP v. $\delta^{18}O$-N_2O slope of ~2 is greater than the ~0.5 produced by N_2O reduction (Lewicka-Szczebak et al., 2017), and, 3) the inverse, rather than parallel, relationship between $\delta^{15}N$-N_2O and $\delta^{18}O$-N_2O rules out N_2O reduction (Snider et al., 2013). Denitrification (or flushing N_2O from denitrifying sediment zones) controlled surface water N_2O when *Q* and hyporheic exchange were high, but as water levels dropped nitrification became the dominant N_2O source. The importance of nitrification was surprising given the high C, low O_2, and high NO_3^- conditions, but adds to similar findings from a hypoxic lake (Salk et al., 2016) to suggest that nitrification-driven N_2O emissions may be more widespread in low O_2 aquatic systems than previously assumed.

4.5 Implications for understanding stream N_2O emissions

Nitrous oxide emissions from the sampled reach were relatively high. Yet the calculated fluxes were between ~ 200% to <50% of those reported from streams with comparable surface water NO_3^- concentrations (Clough et al., 2007; Harrison and Matson, 2003; McMahon and Dennehy, 1999). Notably, the two sites with relatively low N_2O emissions (Clough et al., 2007; Harrison and Matson, 2003) had strong diurnal O_2 and N_2O fluctuations. Turbid and low O_2 waterways like Monaltrie Creek are ubiquitous across the global tropics (Julian et al., 2013) and the Australian continent (Bormans et al., 2004; Oliver et al., 2010). Yet surveying the literature collated here indicates that scientific understanding of stream N_2O (and N) dynamics is primarily based on clear, temperate, northern hemisphere streams < 1 m deep. The role of photoautotrophic N substrate competition in regulating N_2O emissions should be more carefully constrained.

The data here provides direct confirmation of the hypothesis that stream hydrology (opportunity) controls biogenic N_2O emissions (Marzadri et al., 2017; Quick et al., 2016). While many models have been used to assess how flow fluctuations affect stream N cycling (e.g., Azizian et al., 2017; Hester et al., 2019; Rahimi et al., 2015), this study provides one of the first in-situ validations of these interactions. However, while we confirmed that lower flows can make stream reaches become more 'transforming' and less 'transporting' (O'Donnell and Hotchkiss, 2019), we found this shift enhanced NO_3^- and N_2O production rather than removal. Such nitrification-driven N_2O and NO_3^- fluxes has implications for aquatic N_2O modelling: it suggests that the frequently observed positive correlations between NO_3^- and N_2O could reflect microbial coproduction during in-stream nitrification rather than an 'emissions factor' of downstream NO_3^- transport (Kroeze et al., 2005).

Acknowledgements

Research was funded by a Southern Cross University Seed Grant to NSW, with additional support from ARC LP150100519. Invaluable field assistance from: Michelle Simone, Jian-Jhih Chen, Elisabeth Deschaseaux, Charly Moras, Joanne Oakes, Natasha Carlson-Perret, Jessica Riekenberg, and Philip Riekenberg. Paul Kelly & Lea Taylor helped organise and build field equipment. Matheus Carvahlo de Carvahlo, Natasha Carlson-Perret, Iain Alexander, and Dirk Erler assisted with sample analyses. Leslie Jianyin Huang and William Bennett (Griffith University) built the DET probes. Conversations with Marie Kurz (Drexel University) improved the study design and interpretation. **Author contributions:** NSW and BDE conceived the study. NSW carried out the study, with support from volunteers named above. NSW and BDE analysed the data, and NSW wrote the manuscript with input from BDE.

Research data

Data from loggers (including dissolved gas concentrations) and daily sampling (including isotope data) are available for download: https://figshare.com/s/d94125b33e7bd6be5bd8 and https://figshare.com/s/da127a3af8e6c2eeec25. *Note these data links are supplied for reviewing purposes only. Links will be updated to DOIs once the manuscript is accepted.*

Tables

Table 1 Summary of water chemistry recorded during routine monitoring of, 1) surface water at the study site, and, 2) eight groundwater wells installed at either shallow (0.05 m) or deep (0.2 m) depths in the unconfined aquifer between the WWTP and the study site (Fig. 1). Values represent the mean (± SD) of samples collected quarterly over the four years prior to the present study.

	DO	**Conductivity**	**DOC**	**NH_4^+**	**NO_3^-**
	mg l^{-1}	*µS cm^{-1}*	*mg l^{-1}*	*mg N l^{-1}*	*mg N l^{-1}*
Surface water	4.9 (1)	510 (200)	8.4 (5)	0.45 (0.3)	1.4 (1)
Shallow groundwater	2.8 (1)	4,400 (3,000)	17 (10)	0.99 (1)	0.20 (0.4)
Deep groundwater	1.9 (1)	2,700 (1,000)	8.0 (7)	6.7 (6)	0.78 (3)

Table 2 Changes in the $\delta^{18}O$-H_2O composition, temperature (T), conductivity (Cond.), mass ratio of NO_3^- to conductivity (NO_3^-:Cond.), and dissolved organic carbon (DOC) in surface water and hyporheic water collected over three locations along the north bank, centre, and south bank of a stream reach (Fig. 1). Samples were collected at the surface water O_2 maxima and minima* over five days (D1, D2, D4, D6, D8) as stream discharge fell; reported values represent the mean (SD) of six unique samples.

		Surface water					Hyporheic Zone				
		$\delta^{18}O$-H_2O *‰ v. VSMOW*	**T** *°C*	**Cond.** *µS cm^{-1}*	**NO_3^-:Cond.** *µg N µS^{-1}*	**DOC** *mg l^{-1}*	**$\delta^{18}O$-H_2O (c)** *‰ v. VSMOW*	**T** *°C*	**Cond.** *µS cm^{-1}*	**NO_3^-:Cond.** *µg N µS^{-1}*	**DOC** *mg l^{-1}*
D1	North bank	-3.6 (0.06)	21 (0.9)	270 (30)	3.7 (0.9)	1.0 (0.01)	-3.7 (0.7)	23 (1)	710 (70)	0.52 (0.4)	5.9 (2)
	Centre	-3.7 (0.02)		260 (20)	4.7 (0.5)	0.98 (0.07)	-3.6 (0.6)	22 (0.6)	670 (20)	1.2 (0.7)	3.6 (2)
	South bank	-3.7 (0.02)		260 (4)	4.9 (0.2)	0.95 (0.07)	-3.5 (1)	21 (0.1)	670 (20)	1.4 (0.3)	3.3 (2)
D2	North bank	-3.7 (1)	21 (0.3)	270 (10)	5.8 (0.3)	0.94 (0.1)	-4.2 (0.3)	22 (3)	600 (100)	0.25 (0.3)	3.6 (1)
	Centre	-3.7 (0.7)		270 (10)	6.0 (0.3)	0.95 (0.2)	-3.1 (0.9)	23 (0.4)	620 (100)	2.2 (1)	2.2 (0.7)
	South bank	-3.3 (0.8)		280 (6)	6.3 (0.3)	0.89 (0.1)	-3.6 (0.5)	23 (0.4)	600 (70)	2.5 (0.6)	2.0 (1)
D4	North bank	-3.8 (0.5)	22 (0.3)	300 (20)	5.5 (0.5)	0.75 (0.08)	-4.3 (1)	21 (2)	680 (100)	0.08 (0.1)	3.1 (0.7)
	Centre	-3.6 (0.4)		290 (20)	5.6 (0.4)	0.77 (0.05)	-3.8 (0.4)	21 (2)	650 (60)	1.7 (1)	2.0 (0.3)
	South bank	-3.9 (0.3)		280 (60)	7.0 (3)	0.77 (0.02)	-3.9 (0.9)	21 (2)	620 (60)	2.6 (0.7)	2.1 (0.9)
D6	North bank	-4.8 (0.5)	21 (0.5)	300 (9)	6.4 (0.4)	0.78 (0.08)	-5.6 (0.6)	23 (0.9)	1,100 (200)	0.05 (0.03)	9.5 (5)
	Centre	-4.4 (1)		290 (7)	6.4 (0.3)	0.75 (0.03)	-4.9 (0.5)	23 (2)	930 (50)	1.4 (0.9)	2.9 (1)
	South bank	-5.0 (0.7)		300 (10)	6.5 (0.2)	0.75 (0.05)	-4.1 (1)	23 (0.4)	910 (20)	1.7 (0.4)	2.7 (1)
D8	North bank	-4.8 (1)	21 (0.6)	350 (6)	7.1 (0.2)	0.73 (0.05)	-4.4 (0.7)	22 (0.9)	1,700 (200)	0.02 (0.02)	8.9 (2)
	Centre	-4.8 (2)		350 (8)	7.1 (0.2)	0.71 (0.05)	-3.9 (1)	22 (0.7)	1,000 (200)	1.5 (1)	3.5 (2)
	South bank	-4.6 (0.8)		350 (4)	7.1 (0.1)	0.72 (0.05)	-3.0 (2)	22 (1)	1,000 (200)	1.8 (1)	3.5 (3)

*Samples were targeted at night v day (D1 – D4) and low v high tides (D6 – D8)

Table 3: Summary of stream metabolism (productivity / respiration ratio, P/R), the fractional contribution to groundwater to surface water (f_{GW}), and fractional contribution of surface water back into the hyporheic zone (f_{sw}). The P/R ratio was modelled based on surface water O_2 concentrations measured in the centre of the reach (see Suppl. Mat. 2). Values of f_{GW} were calculated using surface water ^{222}Rn concentrations logged in the reach centre, and f_{sw} by comparing conductivity measured twice per sampling date at nine locations in the surface water and 20 cm below the sediment surface (*HZ*) to that of local groundwater, where uncertainty ranges are based on maximum and minimum end-member values (see Suppl. Mat. 3).

Date	P/R	f_{GW}	f_{sw}
D1	0.05	0.35 (0.05 – 0.65)	0.83 (0.73 – 0.87)
D2	0.2	0.32 (0.02 – 0.62)	0.86 (0.75 – 0.92)
D4	0.1	0.54 (0.14 – 0.94)	0.86 (0.75 – 0.91)
D6	0.005	0.58 (0.08 – 1.1)	0.72 (0.51 – 0.82)
D8	0.03	0.61 (0.11 – 1.1)	0.62 (0.24 – 0.82)

Figure captions

Fig. 1 Samples were collected from Monaltrie Creek (b), a tributary of the Wilson River near Lismore, NSW (a). The sampled reach (red box) is downstream of a wastewater treatment plant (WWTP) that discharges inorganic N (DIN) into the surface and groundwater. Samples were collected from the surface water (*SW*), surface sediments (*S*), and deeper hyporheic zone (*HZ*) from the north bank, centre, and south bank of the channel at three locations (b). Shading in (a) represents mean NH_4^+ + NO_3^- concentrations measured during routine monitoring of the shallow groundwater (black triangles) and creek (circles) the year prior to the study; the arrow indicates the groundwater flow direction.

Fig. 2 Changes in surface water conditions over eight days in a highly eutrophic stream in sub-tropical NSW, Australia: (a) stream height and flow velocity, *v*; (b) ^{222}Rn and conductivity; (c) dissolved O_2 (DO) and CO_2; (d) N_2O and NO_3^- concentrations. Parameters were measured over five diurnal cycles (D1, D2, D4, D6, D8). Stream height, *v*, and ^{222}Rn were recorded every 5 min, CO_2 and N_2O every 1 sec, and DO every 15 min. Nitrate concentrations were measured in samples collected from nine locations across the reach twice every 24 h. Gaussian smoothing (black lines) was applied to the *v* and ^{222}Rn data (black points; a, b). Dashed red lines indicate water sampling times.

Fig. 3 Changes the NH_4^+ (a, b, c) and NO_3^- (d, e, f) concentrations of the surface water (*SW*), top 5 cm of the sediments (*S*), and hyporheic zone (*HZ*; 30 cm below the sediment surface) on over an eight-day sampling period (D1 - D8) in a stream reach during falling discharge conditions. Samples were collected from near the north bank, centre, and south bank of the stream at three locations along the reach (water flows A → C). Shaded areas are interpolated between sampling points (black circles; $n = 2$). Note different scale for *S* NH_4^+ concentrations

630 (*), and the exaggerated vertical scale. See Suppl. Mat. Tables S5 – S7 for D2 and D6 data
631 and Suppl. Mat Table S8 for outputs from statistical tests.
632
633 **Fig. 4** The NO_3^- isotopic composition ($\delta^{15}N\text{-}NO_3^-$ v. $\delta^{18}O\text{-}NO_3^-$) in the surface water (*SW*: a,
634 b, c), surface sediments (*S*: d, e, f) and hyporheic zone (*HZ*: g, h, i) of a subtropical stream
635 over eight days of falling water levels (from D1, black circles, to D8, light grey circles).
636 Samples were collected near the north bank (a, d, g), centre (b, e, h), and south bank (c, f, i).
637 Points represent the mean (± SD) of samples from three locations along the length of the 30
638 m reach, which were collected twice over each 24 h period (n = 6). Coloured rectangles show
639 the mean ± SD range for the whole sampling period. Mixed model analysis (F and p values)
640 for $\delta^{18}O\text{-}NO_3^-$ and $\delta^{15}N\text{-}NO_3^-$ variations over the stream width and time are shown.
641
642 **Fig. 5** The $\delta^{15}N\text{-}NO_3^-$ (a), $\delta^{18}O\text{-}NO_3^-$ (b), and NO_3^- concentrations (c) at 5 cm and 20 cm
643 depth in the sediments (brown) and in the surface water (blue), as measured during high flow
644 conditions (D1) and then eight days later after water levels fell (D8). Dashed lines in (b)
645 indicate the theoretical $\delta^{18}O\text{-}NO_3^-$ composition produced from in-situ nitrification (S1:
646 mixing 2×O-H_2O and 1×O-O_2; S2: mixing + kinetic fractionation; outputs from S3, mixing +
647 kinetic fractionation + exchange fell below the scale of the plot). Surface water N_2O
648 concentrations (mean ± SD over three hours around each sampling point) are also shown (c).
649
650 **Fig. 6** The isotopic composition of surface water N_2O, measured five times over eight days as
651 stream flow declined (D1 → D8). Each $\delta^{15}N\text{-}N_2O$, $\delta^{18}O\text{-}N_2O$ and ^{15}N site preference (SP)
652 value represent the mean ± SD of samples collected at nine locations across the width and
653 length of a stream reach; measurements were carried out twice during each 24-hr period. The
654 $\delta^{18}O\text{-}N_2O$ values are corrected for mixing with atmospheric N_2O (Eq. 1); crosses represent

655 uncorrected values. Solid lines represent the best-fit of the linear regression between $\delta^{18}O$-
656 N_2O and SP (a; y = -56 + 1.3x, $p<0.001$, $r^2 = 0.61$) and $\delta^{15}N$-N_2O and $\delta^{18}O$-N_2O (b; y = 16 –
657 0.26x, $p<0.001$, $r^2 = 0.45$), with grey shading over the 95% CI. Dashed lines indicate the SP
658 v $\delta^{18}O$-N_2O (a) and $\delta^{15}N$-N_2O v $\delta^{18}O$-N_2O (b) relationships produced during N_2O reduction
659 to N_2 (Lewicka-Szczebak et al., 2017; Ostrom et al., 2007). The mean surface water N_2O
660 saturation for the three hours around each sampling point is shown (blue points and line).
661
662 **Fig. 7** Over eight days the surface water depth and discharge (*Q*) decreased, causing surface
663 waters to become more groundwater (yellow) dominated as it returned toward baseflow, and
664 less surface water (brown) reached the hyporheic sediment zone (orange). The combination
665 of decreased exchange and increased residence time enhanced biological oxidation of the
666 large sediment NH_4^+ pool, increasing water-air N_2O emissions and downstream NO_3^-
667 discharge. Photos are from two days prior to D1 (left) and on D6 (right), credit: N.S. Wells.
668
669
670
671
672
673
674
675
676
677
678
679

Figures

Figure 1:

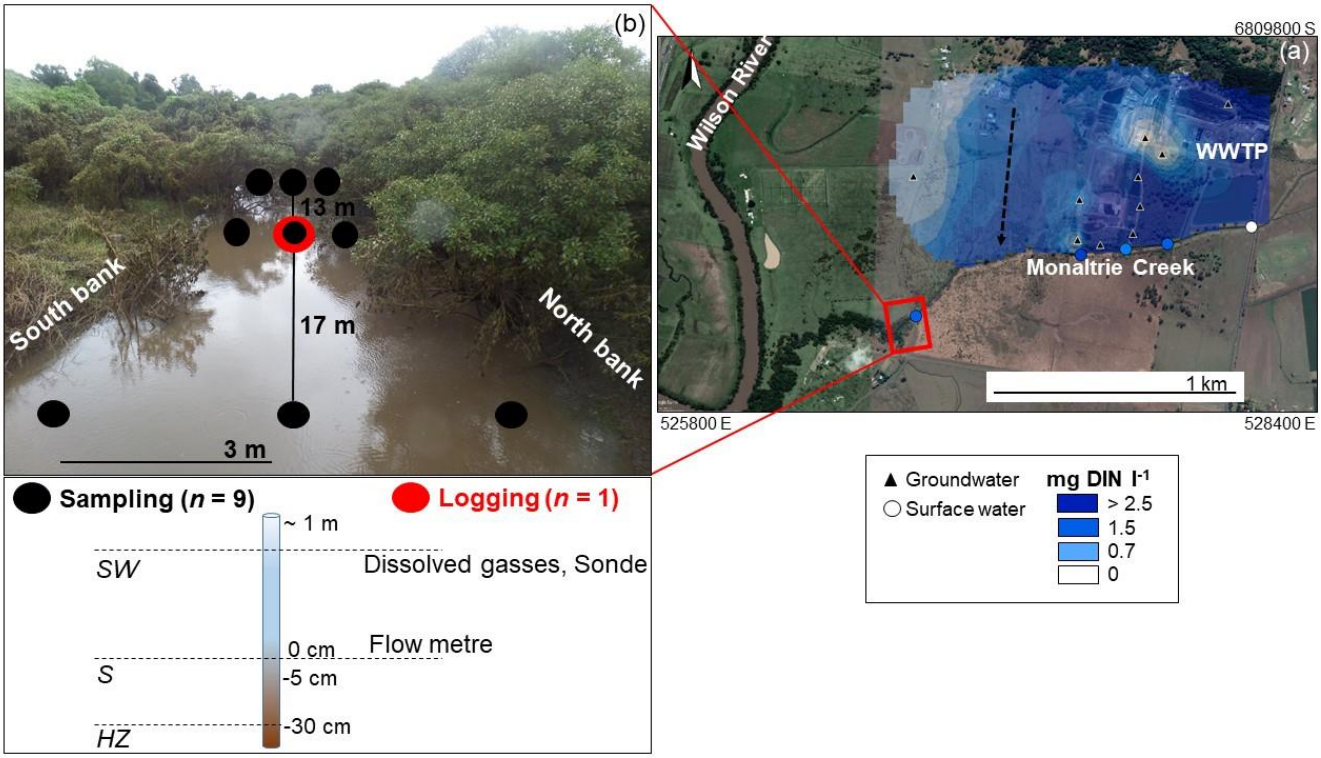

Fig. 1 Samples were collected from Monaltrie Creek (b), a tributary of the Wilson River near Lismore, NSW (a). The sampled reach (red box) is downstream of a wastewater treatment plant (WWTP) that discharges inorganic N (DIN) into the surface and groundwater. Samples were collected from the surface water (*SW*), surface sediments (*S*), and deeper hyporheic zone (*HZ*) from the north bank, centre, and south bank of the channel at three locations (b). Shading in (a) represents mean NH_4^+ + NO_3^- concentrations measured during routine monitoring of the shallow groundwater (black triangles) and creek (circles) the year prior to the study; the arrow indicates the groundwater flow direction.

Figure 2

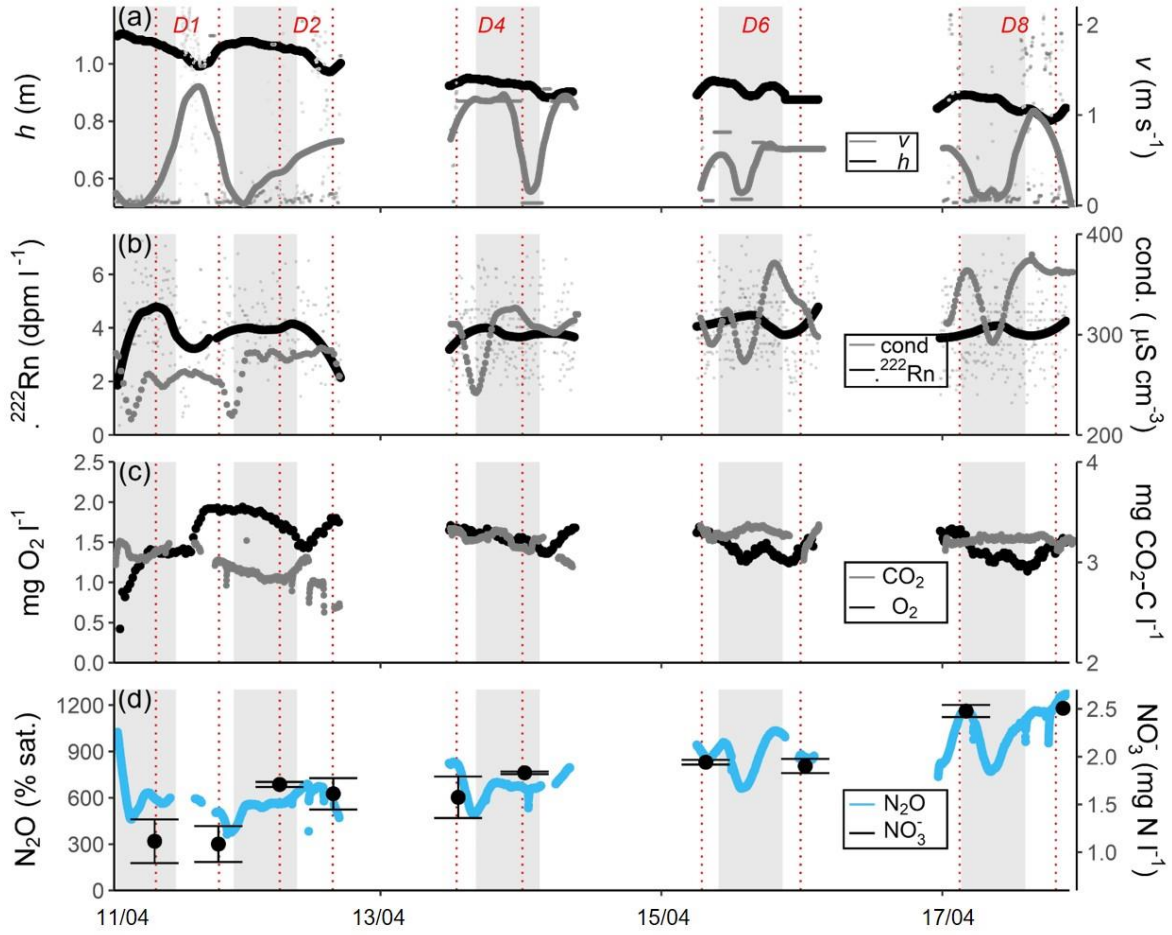

Fig. 2 Changes in surface water conditions over eight days in a highly eutrophic stream in sub-tropical NSW, Australia: (a) stream height and flow velocity, *v*; (b) ^{222}Rn and conductivity; (c) dissolved O_2 (DO) and CO_2; (d) N_2O and NO_3^- concentrations. Parameters were measured over five diurnal cycles (D1, D2, D4, D6, D8). Stream height, *v*, and ^{222}Rn were recorded every 5 min, CO_2 and N_2O every 1 sec, and DO every 15 min. Nitrate concentrations were measured in samples collected from nine locations across the reach twice every 24 h. Gaussian smoothing (black lines) was applied to the *v* and ^{222}Rn data (black points; a, b). Dashed red lines indicate water sampling times.

Figure 3

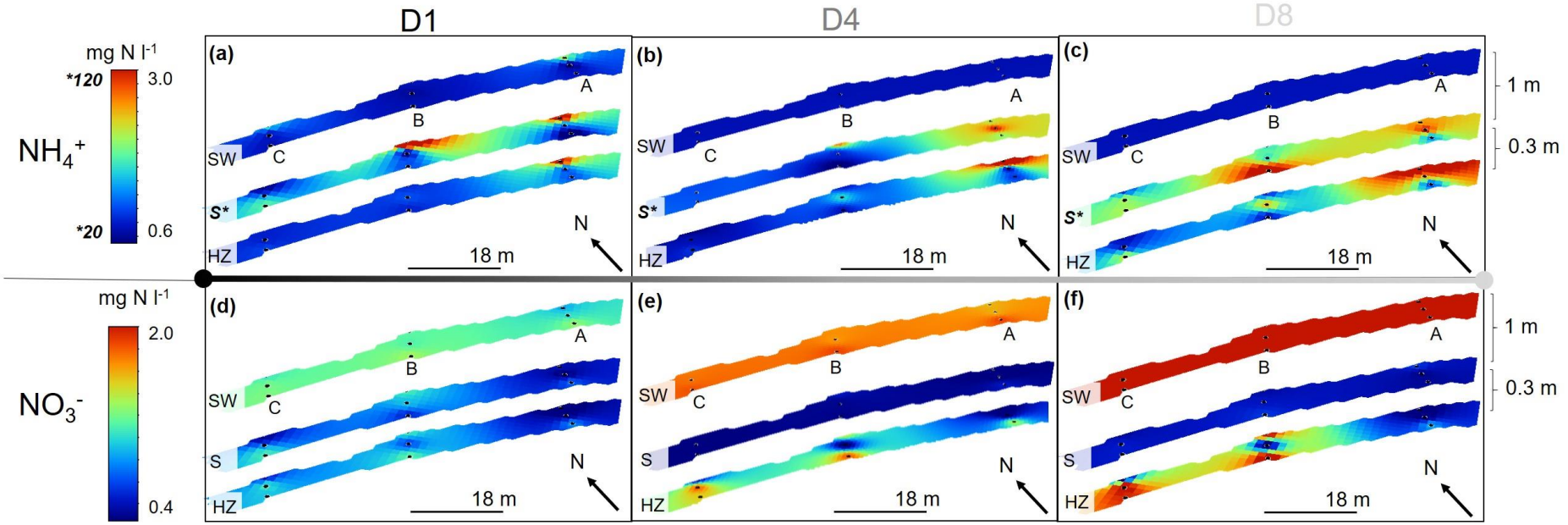

Fig. 3 Changes in NH_4^+ (a, b, c) and NO_3^- (d, e, f) concentrations of the surface water (*SW*), top 5 cm of the sediments (*S*), and hyporheic zone (*HZ*; 30 cm below the sediment surface) on over an eight-day sampling period (D1 - D8) in a stream reach during falling discharge conditions. Samples were collected from near the north bank, centre, and south bank of the stream at three locations along the reach (water flows A → C). Shaded areas are interpolated between sampling points (black circles; $n = 2$). Note the difference in scale for *S* NH_4^+ concentrations (*), and the exaggerated vertical scale. See Suppl. Mat. Tables S5 – S7 for D2 and D6 data and Suppl. Mat Table S8 for outputs from statistical tests.

712 *Figure 4*

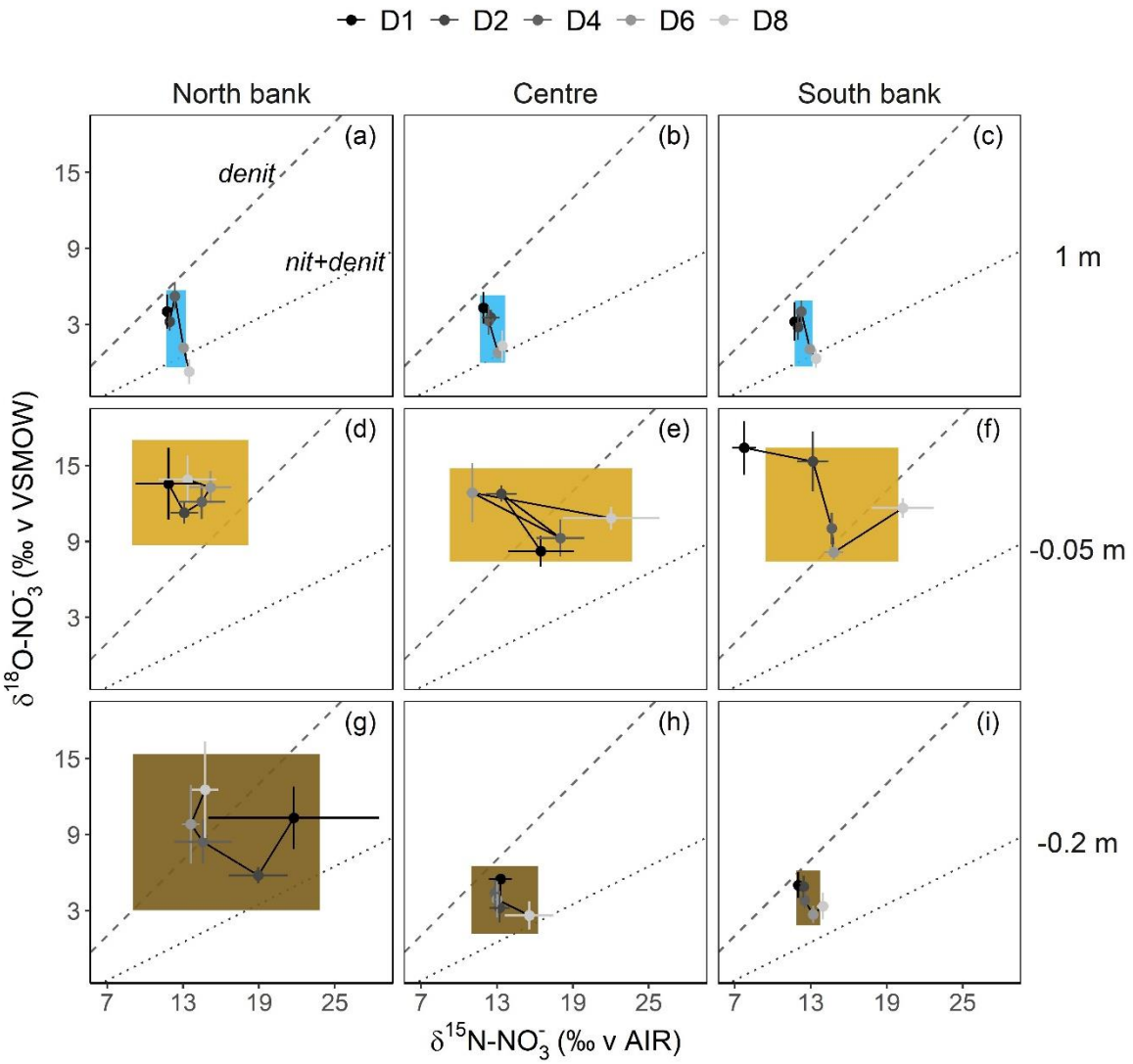

713

714 **Fig. 4** The NO_3^- isotopic composition ($\delta^{15}N\text{-}NO_3^-$ v. $\delta^{18}O\text{-}NO_3^-$) in the surface water (1 m: a,

715 b, c), surface sediments (-0.05 m: d, e, f) and hyporheic zone (-0.2 m: g, h, i) of a stream

716 reach over eight days (D1, black circles, to D8, light grey circles) of falling *Q*. Points

717 represent the mean (± SE) of samples collected twice over each 24 h period from three

718 locations along the 30 m reach, which were (n = 6) across the width of the stream: along the

719 north bank closest to the pollution source (a, d, g), centre (b, e, h), and south bank (c, f, i).

720 Coloured rectangles show the mean ± SD range for the whole sampling period. See Suppl.

721 Mat Table S8 for associated mixed model results.

722

Figure 5

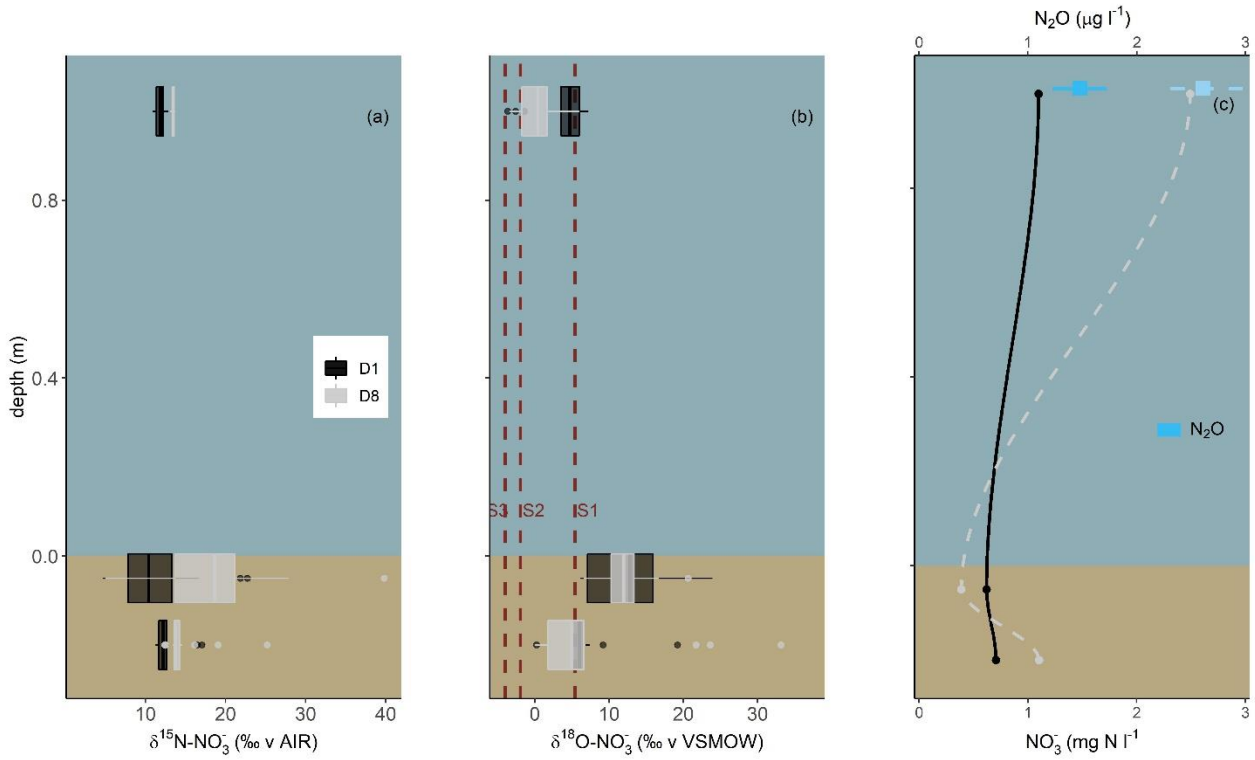

Fig. 5 The $\delta^{15}N\text{-}NO_3^-$ (a), $\delta^{18}O\text{-}NO_3^-$ (b), and NO_3^- concentrations (c) at 5 cm and 20 cm depth in the sediments (brown) and in the surface water (blue), as measured during high flow conditions (D1) and then eight days later after water levels fell (D8). Dashed lines in (b) indicate theoretical $\delta^{18}O\text{-}NO_3^-$ composition produced from in-situ nitrification (S1: mixing $2\times O\text{-}H_2O$ and $1\times O\text{-}O_2$; S2: mixing + kinetic fractionation; S3: mixing + kinetic fractionation + exchange produce $\delta^{18}O\text{-}NO_3^-$ equal to surrounding $\delta^{18}O\text{-}H_2O$). Surface water N_2O concentrations (mean ± SD over three hours around each sampling point) are also shown (c).

Figure 6

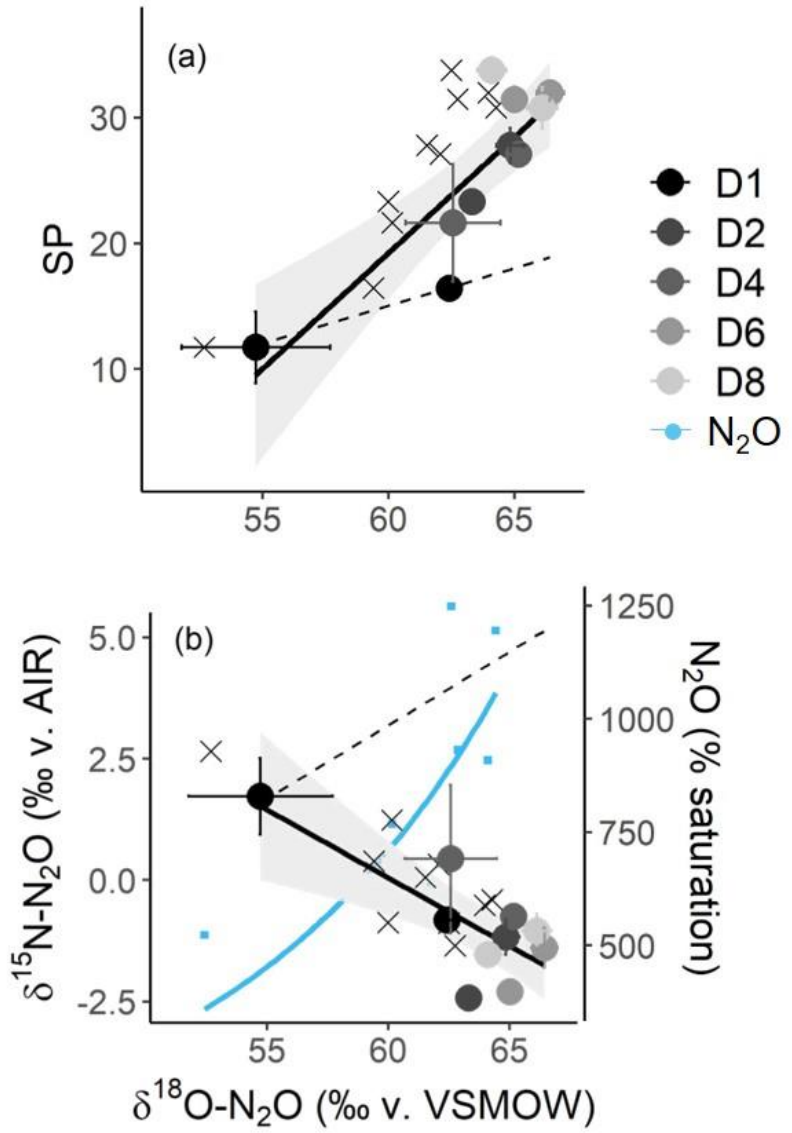

Fig. 6 The isotopic composition of surface water N_2O, measured over eight days as stream flow declined (D1 → D8). Each $\delta^{15}N\text{-}N_2O$, $\delta^{18}O\text{-}N_2O$ and ^{15}N site preference (SP) value represent the mean ± SD of samples collected at nine locations across the width and length of a stream reach; measurements were carried out twice during each 24-hr period. The $\delta^{18}O\text{-}N_2O$ values are corrected for mixing with atmospheric N_2O (Eq. 1); crosses represent uncorrected values. Solid lines represent the best-fit of the linear regression between $\delta^{18}O\text{-}N_2O$ and SP (a; y = -56 + 1.3x, $p<0.001$, $r^2 = 0.61$) and $\delta^{15}N\text{-}N_2O$ and $\delta^{18}O\text{-}N_2O$ (b; y = 16 – 0.26x, $p<0.001$, $r^2 = 0.45$), with grey shading over the 95% CI. Dashed lines indicate the SP v $\delta^{18}O\text{-}N_2O$ (a) and $\delta^{15}N\text{-}N_2O$ v $\delta^{18}O\text{-}N_2O$ (b) relationships produced during N_2O reduction to N_2 (Lewicka-Szczebak et al., 2017; Ostrom et al., 2007). The mean surface water N_2O saturation for the three hours around each sampling point is shown (blue points and line).

Figure 7

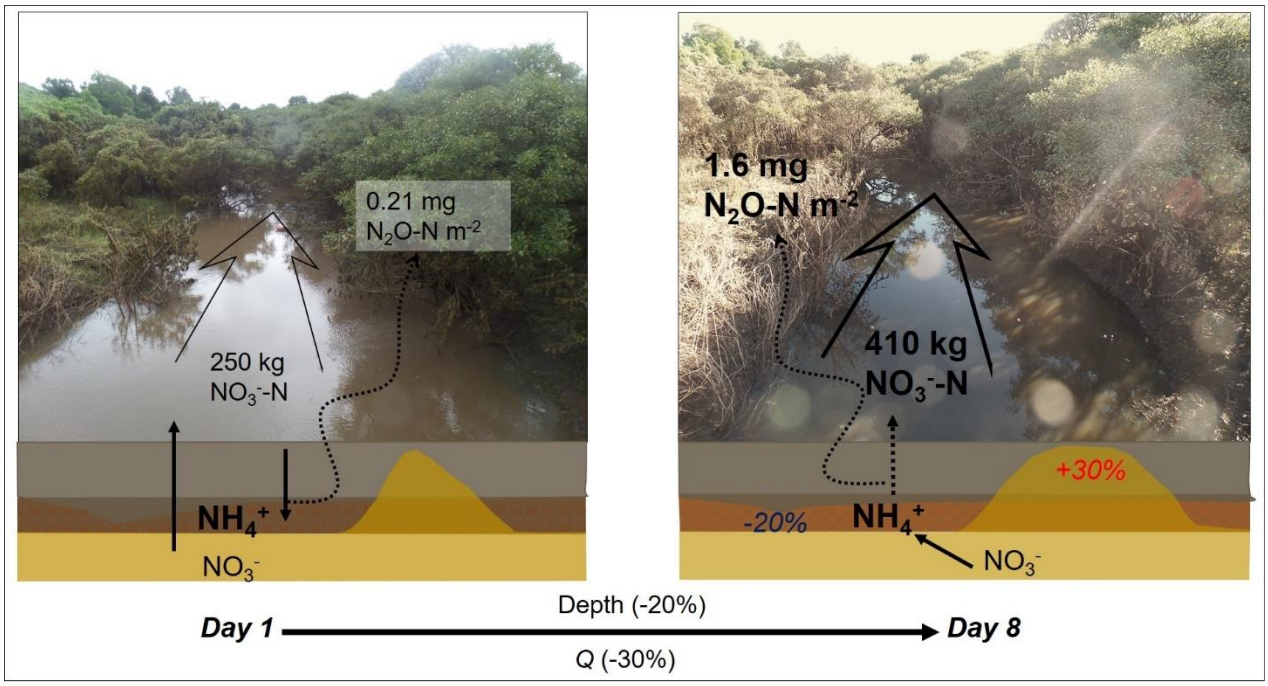

Fig. 7 Over eight days the surface water depth and discharge (*Q*) decreased, causing surface waters to become more groundwater (yellow) dominated as it returned toward baseflow, and less surface water (brown) reached the hyporheic sediment zone (orange). The combination of decreased exchange and increased residence time enhanced biological oxidation of the large sediment NH_4^+ pool, increasing water-air N_2O emissions and downstream NO_3^- discharge. Photos are from two days prior to D1 (left) and on D6 (right), credit: N.S. Wells.

References

Alexander, R.B., Bohlke, J.K., Boyer, E.W., David, M.B., Harvey, J.W., Mulholland, P.J., Seitzinger, S.P., Tobias, C.R., Tonitto, C. and Wollheim, W.M. (2009) Dynamic modeling of nitrogen losses in river networks unravels the coupled effects of hydrological and biogeochemical processes. *Biogeochem.* **93**, 91-116.

Appling, A.P., Hall Jr., R.O., Yackulic, C.B. and Arroita, M. (2018) Overcoming equifinality: Leveraging long time series for stream metabolism estimation. *J. Geophys. Res- Biogeosci.* **123**, 624-645.

Appling, A.P. and Heffernan, J.B. (2014) Nutrient limitation and physiology mediate the fine-scale (de)coupling of biogeochemical cycles. *Am. Nat.* **184**, 384-406.

Atkins, M.L., Santos, I.R., Ruiz-Halpern, S. and Maher, D.T. (2013) Carbon dioxide dynamics driven by groundwater discharge in a coastal floodplain creek. *J. Hydrol.* **493**, 30-42.

Azizian, M., Boano, F., Cook, P.L.M., Detwiler, R.L., Rippy, M.A. and Grant, S.B. (2017) Ambient groundwater flow diminishes nitrate processing in the hyporheic zone of streams. *Water Resour. Res.* **53**, 3941-3967.

Barnes, R.T., Sawyer, A.H., Tight, D.M., Wallace, C.D. and Hastings, M.G. (2019) Hydrogeologic controls of surface water-groundwater nitrogen dynamics within a tidal freshwater zone. *J. Geophys. Res- Biogeosci.* **124**.

Bates, D., Mächler, M., Bolker, B. and Walker, S. (2015) Fitting linear mixed-effects models using lme4. *Journal of Statistical Software* **67**, 48.

Baulch, H.M., Dillon, P.J., Maranger, R., Venkiteswaran, J.J., Wilson, H.F. and Schiff, S.L. (2012) Night and day: short-term variation in nitrogen chemistry and nitrous oxide emissions from streams. *Freshwater Biol.* **57**, 509-525.

Beaulieu, J.J., Tank, J.L., Hamilton, S.K., Wollheim, W.M., Hall, R.O., Mulholland, P.J., Peterson, B.J., Ashkenas, L.R., Cooper, L.W., Dahm, C.N., Dodds, W.K., Grimm, N.B., Johnson, S.L., McDowell, W.H., Poole, G.C., Valett, H.M., Arango, C.P., Bernot, M.J., Burgin, A.J., Crenshaw, C.L., Helton, A.M., Johnson, L.T., O'Brien, J.M., Potter, J.D., Sheibley, R.W., Sobota, D.J. and Thomas, S.M. (2011) Nitrous oxide emission from denitrification in stream and river networks. *P. Natl. Acad. Sci. USA* **108**, 214-219.

Bernhardt, E.S., Heffernan, J.B., Grimm, N.B., Stanley, E.H., Harvey, J.W., Arroita, M., Appling, A.P., Cohen, M.J., McDowell, W.H., Hall, R.O., Read, J.S., Roberts, B.J., Stets, E.G. and Yackulic, C.B. (2018) The metabolic regimes of flowing waters. *Limnol. Oceanograph.* **63**, S99-S118.

Bianchin, M.S., Smith, L. and Beckie, R.D. (2011) Defining the hyporheic zone in a large tidally influenced river. *J. Hydrol.* **406**, 16-29.

Bormans, M., Ford, P.W., Fabbro, L. and Hancock, G. (2004) Onset and persistence of cyanobacterial blooms in a large impounded tropical river, Australia. *Marine and Freshwater Research* **55**, 1-15.

Boshers, D.S., Granger, J., Tobias, C.R., Böhlke, J.K. and Smith, R.L. (2019) Constraining the oxygen isotopic composition of nitrate produced by nitrification. *Environ. Sci. Technol.* **53**, 1206-1216.

Boyer, E.W., Howarth, R.W., Galloway, J.N., Dentener, F.J., Green, P.A. and Vörösmarty, C.J. (2006) Riverine nitrogen export from the continents to the coasts. *Global Biogeochem. Cy.* **20**, n/a-n/a.

Briggs, M.A., Day-Lewis, F.D., Zarnetske, J.P. and Harvey, J.W. (2015) A physical explanation for the development of redox microzones in hyporheic flow. *Geophysical Research Letters* **42**, 4402-4410.

Briggs, M.A., Lautz, L.K. and Hare, D.K. (2014) Residence time control on hot moments of net nitrate production and uptake in the hyporheic zone. *Hydrol. Process.* **28**, 3741-3751.

Brodie, R., Sundaram, B., Tottenham, R., Hostetler, S. and Ransley, T. (2007) An overview of tools for assessing groundwater-surface water connectivity Bureau of Rural Sciences. Bureau of Rural Sciences, Canberra

Brodie, R.S., Green, R. and Graham, M. (2003) Mapping groundwater-dependent ecosystems: a case study in the fractured basalt aquifers of the Alstonville Plateau, New South Wales, Australia.
Buchwald, C., Santoro, A.E., McIlvin, M.R. and Casciotti, K.L. (2012) Oxygen isotopic composition of nitrate and nitrite produced by nitrifying cocultures and natural marine assemblages. *Limnol. Oceanograph.* **57**, 1361-1375.
Burnett, W.C., Peterson, R.N., Santos, I.R. and Hicks, R.W. (2010) Use of automated radon measurements for rapid assessment of groundwater flow into Florida streams. *J. Hydrol.* **380**, 298-304.
Call, M., Maher, D.T., Santos, I.R., Ruiz-Halpern, S., Mangion, P., Sanders, C.J., Erler, D.V., Oakes, J.M., Rosentreter, J., Murray, R. and Eyre, B.D. (2015) Spatial and temporal variability of carbon dioxide and methane fluxes over semi-diurnal and spring-neap-spring timescales in a mangrove creek. *Geochim Cosmochim Ac* **150**, 211-225.
Casciotti, K.L., Sigman, D.M. and Ward, B.B. (2003) Linking diversity and stable isotope fractionation in ammonia-oxidizing bacteria. *Geomicrobiol. J.* **20**, 335-353.
Chamberlin, C.A., Bernhardt, E.S., Rosi, E.J. and Heffernan, J.B. (2019) Stoichiometry and daily rhythms: experimental evidence shows nutrient limitation decouples N uptake from photosynthesis. *Ecology* **100**, e02822.
Chen, X.L., Tague, C.L., Melack, J.M. and Keller, A.A. (2020) Sensitivity of nitrate concentration-discharge patterns to soil nitrate distribution and drainage properties in the vertical dimension. *Hydrol. Process.*, 17.
Christensen, P.B., Nielsen, L.P., Sorensen, J. and Revsbech, N.P. (1990) Denitrification in nitrate-rich streams - Diurnal and seasonal - variation related to benthic oxygen-metabolism. *Limnol. Oceanograph.* **35**, 640-651.
Clough, T.J., Buckthought, L.E., Kelliher, F.M. and Sherlock, R.R. (2007) Diurnal fluctuations of dissolved nitrous oxide (N_2O) concentrations and estimates of N_2O emissions from a spring-fed river: implications for IPCC methodology. *Global Change Biol.* **13**, 1016-1027.
Cohen, M.J., Heffernan, J.B., Albertin, A. and Martin, J.B. (2012) Inference of riverine nitrogen processing from longitudinal and diel variation in dual nitrate isotopes. *J. Geophys. Res.-Biogeosci.* **117**, 17.
Comer-Warner, S., Knapp, J.L.A., Blaen, P., Klaar, M., Shelley, F., Zarnetske, J., Lee-Cullin, J., Folegot, S., Kurz, M., Lewandowski, J., Harvey, J., Ward, A., Mendoza-Lera, C., Ullah, S., Datry, T., Kettridge, N., Gooddy, D., Drummond, J., Martí, E., Milner, A., Hannah, D. and Krause, S. (2020a) The method controls the story - Sampling method impacts on the detection of pore-water nitrogen concentrations in streambeds. *Sci. Total Environ.* **709**, 136075.
Comer-Warner, S.A., Gooddy, D.C., Ullah, S., Glover, L., Kettridge, N., Wexler, S.K., Kaiser, J. and Krause, S. (2020b) Seasonal variability of sediment controls of nitrogen cycling in an agricultural stream. *Biogeochem.* **148**, 31-48.
Comer-Warner, S.A., Krause, S., Gooddy, D.C., Bennett, S.A., Wexler, S.K. and Kaiser, J. (2017) Opening opportunities for high-resolution isotope analysis - Quantification of delta N-15(NO3) and delta O-18(NO3) in diffusive equilibrium in thin-film passive samplers. *Anal. Chem.* **89**, 4139-4146.
Covino, T.P., Bernhardt, E.S. and Heffernan, J.B. (2018) Measuring and interpreting relationships between nutrient supply, demand, and limitation. *Freshwater Sci.* **37**, 448-455.
Denk, T.R.A., Mohn, J., Decock, C., Lewicka-Szczebak, D., Harris, E., Butterbach-Bahl, K., Kiese, R. and Wolf, B. (2017) The nitrogen cycle: A review of isotope effects and isotope modeling approaches. *Soil Biol. Biochem.* **105**, 121-137.
Dudley-Southern, M. and Binley, A. (2015) Temporal responses of groundwater-surface water exchange to successive storm events. *Water Resour. Res.* **51**, 1112-1126.
Erler, D.V., Duncan, T.M., Murray, R., Maher, D.T., Santos, I.R., Gatland, J.R., Mangion, P. and Eyre, B.D. (2015) Applying cavity ring-down spectroscopy for the measurement of dissolved nitrous oxide concentrations and bulk nitrogen isotopic composition in aquatic systems: Correcting for interferences and field application. *Limnology & Oceanography: Methods* **13**, 391-401.
Eyre, B.D. and Ferguson, A.J.P. (2009) Denitrification efficiency for defining critical loads of carbon in shallow coastal ecosystems. *Hydrobiologia* **629**, 137-146.

Eyre, B.D. and Pont, D. (2003) Intra- and inter-annual variability in the different forms of diffuse nitrogen and phosphorus delivered to seven sub-tropical east Australian estuaries. *Estuarine, Coastal and Shelf Science* **57**, 137-148.

Fang, Y., Koba, K., Makabe, A., Zhu, F., Fan, S., Liu, X. and Yoh, M. (2012) Low $\delta^{18}O$ values of nitrate produced from nitrification in temperate forest soils. *Environ. Sci. Technol.* **46**, 8723-8730.

Fork, M.L. and Heffernan, J.B. (2014) Direct and indirect effects of dissolved organic matter source and concentration on denitrification in northern Florida rivers. *Ecosystems* **17**, 14-28.

Fowler, D., Coyle, M., Skiba, U., Sutton, M.A., Cape, J.N., Reis, S., Sheppard, L.J., Jenkins, A., Grizzetti, B., Galloway, J.N., Vitousek, P., Leach, A., Bouwman, A.F., Butterbach-Bahl, K., Dentener, F., Stevenson, D., Amann, M. and Voss, M. (2013) The global nitrogen cycle in the twenty-first century. *Philosophical Transactions of the Royal Society B: Biological Sciences* **368**, 20130164.

Frame, C.H. and Casciotti, K.L. (2010) Biogeochemical controls and isotopic signatures of nitrous oxide production by a marine ammonia-oxidizing bacterium. *Biogeosci.* **7**, 2695-2709.

Galloway, J.N., Townsend, A.R., Erisman, J.W., Bekunda, M., Cai, Z., Freney, J.R., Martinelli, L.A., Seitzinger, S.P. and Sutton, M.A. (2008) Transformation of the nitrogen cycle: Recent trends, questions, and potential solutions. *Science* **320**, 889-892.

Gatland, J.R., Santos, I.R., Maher, D.T., Duncan, T.M. and Erler, D.V. (2014) Carbon dioxide and methane emissions from an artificially drained coastal wetland during a flood: Implications for wetland global warming potential. *J. Geophys. Res.-Biogeosci.* **119**, 1698-1716.

Gomez-Velez, J.D., Harvey, J., Cardenas, M.B. and Kiel, B. (2015) Denitrification in the Mississippi River network controlled by flow through river bedforms. *Nat. Geosci.* **8**, 941-U975.

Granger, J. and Wankel, S.D. (2016) Isotopic overprinting of nitrification on denitrification as a ubiquitous and unifying feature of environmental nitrogen cycling. *Proc Natl Acad Sci U S A* **113**, E6391-E6400.

Gupta, G. and Karuppiah, M. (1996) Toxicity study of a Chesapeake Bay tributary - Wicomico River. *Chemosphere* **32**, 1193-1215.

Hall, R.O. and Tank, J.L. (2003) Ecosystem metabolism controls nitrogen uptake in streams in Grand Teton National Park, Wyoming. *Limnol. Oceanograph.* **48**, 1120-1128.

Hall, R.O. and Ulseth, A.J. (2019) Gas exchange in streams and rivers. *WIREs Water* **0**, e1391.

Hampton, T.B., Zarnetske, J.P., Briggs, M.A., Dehkordy, F.M., Singha, K., Day-Lewis, F.D., Harvey, J.W., Chowdhury, S.R. and Lane, J.W. (2020) Experimental shifts of hydrologic residence time in a sandy urban stream sediment-water interface alter nitrate removal and nitrous oxide fluxes. *Biogeochem.* **149**, 195–219.

Harrison, J. and Matson, P. (2003) Patterns and controls of nitrous oxide emissions from waters draining a subtropical agricultural valley. *Global Biogeochem. Cy.* **17**, 13.

Harrison, J.A., Matson, P.A. and Fendorf, S.E. (2005) Effects of a diel oxygen cycle on nitrogen transformations and greenhouse gas emissions in a eutrophied subtropical stream. *Aquat. Sci.* **67**, 308-315.

Harvey, J.W., Bohlke, J.K., Voytek, M.A., Scott, D. and Tobias, C.R. (2013) Hyporheic zone denitrification: Controls on effective reaction depth and contribution to whole-stream mass balance. *Water Resour. Res.* **49**, 6298-6316.

Haslun, J.A., Ostrom, N.E., Hegg, E.L. and Ostrom, P.H. (2018) Estimation of isotope variation of N_2O during denitrification by Pseudomonas aureofaciens and Pseudomonas chlororaphis: implications for N_2O source apportionment. *Biogeosci.* **15**, 3873-3882.

Hester, E.T., Eastes, L.A. and Widdowson, M.A. (2019) Effect of surface water stage fluctuation on mixing-dependent hyporheic denitrification in riverbed dunes. *Water Resour. Res.* **55**, 4668-4687.

Hu, M.P., Chen, D.J. and Dahlgren, R.A. (2016) Modeling nitrous oxide emission from rivers: A global assessment. *Global Change Biol.* **22**, 3566-3582.

Huang, J., Bennett, W.W., Welsh, D.T., Li, T. and Teasdale, P.R. (2016) "Diffusive Gradients in Thin Films" techniques provide representative time-weighted average measurements of inorganic nutrients in dynamic freshwater systems. *Environ. Sci. Technol.* **50**, 13446-13454.

Huang, J.Y., Franklin, H., Teasdale, P.R., Burford, M.A., Kankanamge, N.R., Bennett, W.W. and Welsh, D.T. (2019) Comparison of DET, DGT and conventional porewater extractions for determining nutrient profiles and cycling in stream sediments. *Environ. Sci.-Process Impacts* **21**, 2128-2140.

Ji, Q.X., Frey, C., Sun, X., Jackson, M., Lee, Y.S., Jayakumar, A., Cornwell, J.C. and Ward, B.B. (2018) Nitrogen and oxygen availabilities control water column nitrous oxide production during seasonal anoxia in the Chesapeake Bay. *Biogeosci.* **15**, 6127-6138.

Julian, J.P., Davies-Colley, R.J., Gallegos, C.L. and Tran, T.V. (2013) Optical water quality of inland waters: a landscape perspective. *Ann. Assoc. Am. Geogr.* **103**, 309-318.

Kassambara, A. (2020) ggpubr: 'ggplot2' Based Publication Ready Plots, R package version 0.3.0 ed, https://CRAN.R-project.org/package=ggpubr.

Kendall, C. (1998) Tracing nitrogen sources and cycling in catchments, in: Kendall, C., Mcdonell, J.J. (Eds.), Isotope Tracers in Catchment Hydrology. Elsevier Science B.V., Amsterdam, pp. 519-576.

Kessler, A.J., Glud, R.N., Cardenas, M.B. and Cook, P.L.M. (2013) Transport zonation limits coupled nitrification-denitrification in permeable sediments. *Environ. Sci. Technol.* **47**, 13404-13411.

Khadka, M.B., Martin, J.B. and Kurz, M.J. (2017) Synoptic estimates of diffuse groundwater seepage to a spring-fed karst river at high spatial resolution using an automated radon measurement technique. *J. Hydrol.* **544**, 86-96.

Knights, D., Sawyer, A.H., Barnes, R.T., Musial, C.T. and Bray, S. (2017) Tidal controls on riverbed denitrification along a tidal freshwater zone. *Water Resour. Res.* **53**, 799-816.

Knowles, J.E. and Frederick, C. (2019) merTools: Tools for Analyzing Mixed Effect Regression Models, R package version 0.5.0 ed, https://CRAN.R-project.org/package=merTools.

Krause, S., Lewandowski, J., Grimm, N.B., Hannah, D.M., Pinay, G., McDonald, K., Martí, E., Argerich, A., Pfister, L., Klaus, J., Battin, T., Larned, S.T., Schelker, J., Fleckenstein, J., Schmidt, C., Rivett, M.O., Watts, G., Sabater, F., Sorolla, A. and Turk, V. (2017) Ecohydrological interfaces as hotspots of ecosystem processes. *Water Resour. Res.*, n/a-n/a.

Kroeze, C., Dumont, E. and Seitzinger, S.P. (2005) New estimates of global emissions of N_2O from rivers and estuaries. *Environmental Sciences* **2**, 159-165.

Kroopnick, P. and Craig, H. (1972) Atmospheric oxygen: isotopic composition and solubility fractionation. *Science* **175**, 54-55.

Laursen, A.E. and Seitzinger, S.P. (2004) Diurnal patterns of denitrification, oxygen consumption and nitrous oxide production in rivers measured at the whole-reach scale. *Freshwater Biol.* **49**, 1448-1458.

Lewandowski, J., Arnon, S., Banks, E., Batelaan, O., Betterle, A., Broecker, T., Coll, C., Drummond, J.D., Garcia, J.G., Galloway, J., Gomez-Velez, J., Grabowski, R.C., Herzog, S.P., Hinkelmann, R., Hohne, A., Hollender, J., Horn, M.A., Jaeger, A., Krause, S., Prats, A.L., Magliozzi, C., Meinikmann, K., Mojarrad, B.B., Mueller, B.M., Peralta-Maraver, I., Popp, A.L., Posselt, M., Putschew, A., Radke, M., Raza, M., Riml, J., Robertson, A., Rutere, C., Schaper, J.L., Schirmer, M., Schulz, H., Shanafield, M., Singh, T., Ward, A.S., Wolke, P., Worman, A. and Wu, L.W. (2019) Is the hyporheic zone relevant beyond the scientific community? *Water* **11**, 32.

Lewicka-Szczebak, D., Augustin, J., Giesemann, A. and Well, R. (2017) Quantifying N_2O reduction to N_2 based on N_2O isotopocules - validation with independent methods (helium incubation and ^{15}N gas flux method). *Biogeosci.* **14**, 22.

Looman, A., Santos, I.R., Tait, D.R., Webb, J.R., Sullivan, C.A. and Maher, D.T. (2016) Carbon cycling and exports over diel and flood-recovery timescales in a subtropical rainforest headwater stream. *Sci. Total Environ.* **550**, 645-657.

Maher, D.T., Santos, I.R., Leuven, J.R.F.W., Oakes, J.M., Erler, D.V., Carvalho de Carvalho, M. and Eyre, B.D. (2013) Novel use of cavity ring-down spectroscopy to investigate aquatic carbon cycling from microbial to ecosystem scales. *Environ. Sci. Technol.* **47**, 12938-12945.

Marcé, R., von Schiller, D., Aguilera, R., Martí, E. and Bernal, S. (2018) Contribution of hydrologic opportunity and biogeochemical reactivity to the variability of nutrient retention in river networks. *Global Biogeochem. Cy.* **32**, 376-388.

Martí, E., Feijoó, C., Vilches, C., Ferreiro, N., Gantes, P., Ranieri, C., Torremorell, A., Castro, M.C.R., Gultemiriam, M.L., Giorgi, A. and Sabater, F. (2020) Diel variation of nutrient retention is associated with metabolism for ammonium but not phosphorus in a lowland stream. *Freshwater Sci.* **0**, 000-000.

Marzadri, A., Dee, M.M., Tonina, D., Bellin, A. and Tank, J.L. (2017) Role of surface and subsurface processes in scaling N_2O emissions along riverine networks. *Proc Natl Acad Sci U S A* **114**, 4330-4335.

McCrackin, M.L., Harrison, J.A. and Compton, J.E. (2014) Factors influencing export of dissolved inorganic nitrogen by major rivers: A new, seasonal, spatially explicit, global model. *Global Biogeochem. Cy.* **28**, 269-285.

McIlvin, M.R. and Casciotti, K.L. (2011) Technical updates to the bacterial method for nitrate isotopic analyses. *Anal. Chem.* **83**, 1850-1856.

McKee, L., Eyre, B. and Hossain, S. (2000) Intra- and interannual export of nitrogen and phosphorus in the subtropical Richmond River catchment, Australia. *Hydrol. Process.* **14**, 1787-1809.

McMahon, P.B. and Dennehy, K.F. (1999) N_2O emissions from a nitrogen-enriched river. *Environ. Sci. Technol.* **33**, 21-25.

Mohn, J., Wolf, B., Toyoda, S., Lin, C.-T., Liang, M.-C., Brüggemann, N., Wissel, H., Steiker, A.E., Dyckmans, J., Szwec, L., Ostrom, N.E., Casciotti, K.L., Forbes, M., Giesemann, A., Well, R., Doucett, R.R., Yarnes, C.T., Ridley, A.R., Kaiser, J. and Yoshida, N. (2014) Interlaboratory assessment of nitrous oxide isotopomer analysis by isotope ratio mass spectrometry and laser spectroscopy: current status and perspectives. *Rapid Communications in Mass Spectrometry* **28**, 1995-2007.

Morgan, B., Rate, A.W. and Burton, E.D. (2012) Water chemistry and nutrient release during the resuspension of FeS-rich sediments in a eutrophic estuarine system. *Sci. Total Environ.* **432**, 47-56.

Murray, R., Erler, D., Rosentreter, J., Maher, D. and Eyre, B. (2018) A seasonal source and sink of nitrous oxide in mangroves: Insights from concentration, isotope, and isotopomer measurements. *Geochim Cosmochim Ac* **238**, 169-192.

Murray, R.H., Erler, D.V. and Eyre, B.D. (2015) Nitrous oxide fluxes in estuarine environments: Response to global change. *Global Change Biol.* **21**, 3219-3245.

Naranjo, R.C., Niswonger, R.G. and Davis, C.J. (2015) Mixing effects on nitrogen and oxygen concentrations and the relationship to mean residence time in a hyporheic zone of a riffle-pool sequence. *Water Resour. Res.* **51**, 7202-7217.

O'Donnell, B. and Hotchkiss, E.R. (2019) Coupling concentration- and process-discharge relationships integrates water chemistry and metabolism in streams. *Water Resour. Res.* **55**, 12.

Ocampo, C.J., Oldham, C.E., Sivapalan, M. and Turner, J.V. (2006) Hydrological versus biogeochemical controls on catchment nitrate export: a test of the flushing mechanism. *Hydrol. Process.* **20**, 4269-4286.

Oliver, R.L., Mitrovic, S.M. and Rees, C. (2010) Influence of salinity on light conditions and phytoplankton growth in a turbid river. *River Research and Applications* **26**, 894-903.

Ostrom, N.E. and Ostrom, P.H. (2017) Mining the isotopic complexity of nitrous oxide: a review of challenges and opportunities. *Biogeochem.* **132**, 359-372.

Ostrom, N.E., Pitt, A., Sutka, R., Ostrom, P.H., Grandy, A.S., Huizinga, K.M. and Robertson, G.P. (2007) Isotopologue effects during N_2O reduction in soils and in pure cultures of denitrifiers. *J. Geophys. Res.-Biogeosci.* **112**, 12.

Palmer-Felgate, E.J., Mortimer, R.J.G., Krom, M.D. and Jarvie, H.P. (2010) Impact of point-source pollution on phosphorus and nitrogen cycling in stream-bed sediments. *Environ. Sci. Technol.* **44**, 908-914.

Parker, S.R., Poulson, S.R., Gammons, C.H. and DeGrandpre, M.D. (2005) Biogeochemical controls on diel cycling of stable isotopes of dissolved O_2 and dissolved inorganic carbon in the Big Hole River, Montana. *Environ. Sci. Technol.* **39**, 7134-7140.

Pedersen, T.L. (2019) patchwork: The Composer of Plots, R package version 1.0.0 ed, https://CRAN.R-project.org/package=patchwork.

Quick, A.M., Reeder, W.J., Farrell, T.B., Tonina, D., Feris, K.P. and Benner, S.G. (2016) Controls on nitrous oxide emissions from the hyporheic zones of streams. *Environ. Sci. Technol.* **50**, 11491-11500.

Quick, A.M., Reeder, W.J., Farrell, T.B., Tonina, D., Feris, K.P. and Benner, S.G. (2019) Nitrous oxide from streams and rivers: A review of primary biogeochemical pathways and environmental variables. *Earth-Sci. Rev.* **191**, 224-262.

Rahimi, M., Essaid, H.I. and Wilson, J.T. (2015) The role of dynamic surface water-groundwater exchange on streambed denitrification in a first-order, low-relief agricultural watershed. *Water Resour. Res.* **51**, 9514-9538.

Raymond, P.A., Saiers, J.E. and Sobczak, W.V. (2016) Hydrological and biogeochemical controls on watershed dissolved organic matter transport: pulse-shunt concept. *Ecology* **97**, 5-16.

Raymond, P.A., Zappa, C.J., Butman, D., Bott, T.L., Potter, J., Mulholland, P., Laursen, A.E., McDowell, W.H. and Newbold, D. (2012) Scaling the gas transfer velocity and hydraulic geometry in streams and small rivers. *Limnology & Oceanography: Fluids and Environments* **2**, 41-53.

Reading, M.J., Santos, I.R., Maher, D.T., Jeffrey, L. and Tait, D.R. (2017) Shifting nitrous oxide source/sink behaviour in a subtropical estuary revealed by automated time series observations. *Estuarine, Coastal and Shelf Science* **194**, 66-76.

Reisinger, A.J., Doody, T.R., Groffman, P.M., Kaushal, S.S. and Rosi, E.J. (2019) Seeing the light: urban stream restoration affects stream metabolism and nitrate uptake via changes in canopy cover. *Ecol. Appl.* **29**, 15.

Reisinger, A.J., Tank, J.L., Hoellein, T.J. and Hall, R.O. (2016) Sediment, water column, and open-channel denitrification in rivers measured using membrane-inlet mass spectrometry. *J. Geophys. Res.-Biogeosci.* **121**, 1258-1274.

Rosamond, M.S., Thuss, S.J. and Schiff, S.L. (2012) Dependence of riverine nitrous oxide emissions on dissolved oxygen levels. *Nat. Geosci.* **5**, 715.

Rosamond, M.S., Thuss, S.J., Schiff, S.L. and Elgood, R.J. (2011) Coupled cycles of dissolved oxygen and nitrous oxide in rivers along a trophic gradient in southern Ontario, Canada. *J. Environ. Qual.* **40**, 256-270.

Salk, K.R., Ostrom, P.H., Biddanda, B.A., Weinke, A.D., Kendall, S.T. and Ostrom, N.E. (2016) Ecosystem metabolism and greenhouse gas production in a mesotrophic northern temperate lake experiencing seasonal hypoxia. *Biogeochem.* **131**, 303-319.

Santos, I.R., Maher, D.T. and Eyre, B.D. (2012) Coupling automated radon and carbon dioxide measurements in coastal waters. *Environ. Sci. Technol.* **46**, 7685-7691.

Schubert, M. and Paschke, A. (2015) Radon, CO_2 and CH_4 as environmental tracers in groundwater/surface water interaction studies - comparative theoretical evaluation of the gas specific water/air phase transfer kinetics. *Eur. Phys. J.-Spec. Top.* **224**, 709-715.

Schutte, C.A., Joye, S.B., Wilson, A.M., Evans, T., Moore, W.S. and Casciotti, K. (2015) Intense nitrogen cycling in permeable intertidal sediment revealed by a nitrous oxide hot spot. *Global Biogeochem. Cy.* **29**, 1584-1598.

Seitzinger, S., Harrison, J.A., Bohlke, J.K., Bouwman, A.F., Lowrance, R., Peterson, B., Tobias, C. and Van Drecht, G. (2006) Denitrification across landscapes and waterscapes: A synthesis. *Ecol. Appl.* **16**, 2064-2090.

Singh, T., Wu, L.W., Gomez-Velez, J.D., Lewandowski, J., Hannah, D.M. and Krause, S. (2019) Dynamic hyporheic zones: exploring the role of peak flow events on bedform-induced hyporheic exchange. *Water Resour. Res.* **55**, 218-235.

Smith, J.M., Chavez, F.P. and Francis, C.A. (2014) Ammonium uptake by phytoplankton regulates nitrification in the sunlit ocean. *PloS one* **9**, 9.

Snider, D.M., Schiff, S.L. and Spoelstra, J. (2009) N-15/N-14 and O-18/O-16 stable isotope ratios of nitrous oxide produced during denitrification in temperate forest soils. *Geochim Cosmochim Ac* **73**, 877-888.

Snider, D.M., Venkiteswaran, J.J., Schiff, S.L. and Spoelstra, J. (2013) A new mechanistic model of $\delta^{18}O$-N_2O formation by denitrification. *Geochim Cosmochim Ac* **112**, 102-115.

Stanley, E.H., Casson, N.J., Christel, S.T., Crawford, J.T., Loken, L.C. and Oliver, S.K. (2016) The ecology of methane in streams and rivers: patterns, controls, and global significance. *Ecol. Monogr.* **86**, 146-171.

Stephens, B.M., Wankel, S.D., Beman, J.M., Rabines, A.J., Allen, A.E. and Aluwihare, L.I. (2019) Euphotic zone nitrification in the California Current Ecosystem. *Limnol. Oceanograph.* **9999**, 1-17.

Tank, J.L., Rosi-Marshall, E.J., Griffiths, N.A., Entrekin, S.A. and Stephen, M.L. (2010) A review of allochthonous organic matter dynamics and metabolism in streams. *J. N. Am. Benthol. Soc.* **29**, 118-146.

Thuss, S.J., Venkiteswaran, J.J. and Schiff, S.L. (2014) Proper interpretation of dissolved nitrous oxide isotopes, production pathways, and emissions requires a modelling approach. *PloS one* **9**, 15.

Toyoda, S. and Yoshida, N. (1999) Determination of nitrogen isotopomers of nitrous oxide on a modified isotope ratio mass spectrometer. *Anal. Chem.* **71**, 4711-4718.

Trauth, N. and Fleckenstein, J.H. (2017) Single discharge events increase reactive efficiency of the hyporheic zone. *Water Resour. Res.* **53**, 779-798.

Trauth, N., Schmidt, C., Vieweg, M., Maier, U. and Fleckenstein, J.H. (2014) Hyporheic transport and biogeochemical reactions in pool-riffle systems under varying ambient groundwater flow conditions. *J. Geophys. Res.-Biogeosci.* **119**, 910-928.

Trimmer, M., Grey, J., Heppell, C.M., Hildrew, A.G., Lansdown, K., Stahl, H. and Yvon-Durocher, G. (2012) River bed carbon and nitrogen cycling: State of play and some new directions. *Sci. Total Environ.* **434**, 143-158.

Turner, P.A., Griffis, T.J., Lee, X.H., Baker, J.M., Venterea, R.T. and Wood, J.D. (2015) Indirect nitrous oxide emissions from streams within the US Corn Belt scale with stream order. *Proc Natl Acad Sci U S A* **112**, 9839-9843.

Tysmans, D.J.J., Lohr, A.J., Kroeze, C., Ivens, W. and van Wijnen, J. (2013) Spatial and temporal variability of nutrient retention in river basins: A global inventory. *Ecol. Indic.* **34**, 607-615.

Venkiteswaran, J.J., Rosamond, M.S. and Schiff, S.L. (2014) Nonlinear response of riverine N_2O fluxes to oxygen and temperature. *Environ. Sci. Technol.* **48**, 1566-1573.

Wanninkhof, R. (2014) Relationship between wind speed and gas exchange over the ocean revisited. *Limnology & Oceanography: Methods* **12**, 351-362.

Webb, J.R., Santos, I.R., Robson, B., Macdonald, B., Jeffrey, L. and Maher, D.T. (2017) Constraining the annual groundwater contribution to the water balance of an agricultural floodplain using radon: The importance of floods. *Water Resour. Res.* **53**, 544-562.

Weiss, R.F. and Price, B.A. (1980) Nitrous-oxide solubility in water and seawater. *Mar. Chem.* **8**, 347-359.

Well, R., Eschenbach, W., Flessa, H., von der Heide, C. and Weymann, D. (2012) Are dual isotope and isotopomer ratios of N_2O useful indicators for N_2O turnover during denitrification in nitrate-contaminated aquifers? *Geochim Cosmochim Ac* **90**, 265-282.

Wells, N.S., Baisden, W.T., Clough, T.J., Johnson-Beebout, S.E. and Elberling, B. (2019) Effects of denitrification and transport on the isotopic composition of nitrate ($\delta^{18}O$, $\delta^{15}N$) in freshwater systems. *Sci. Total Environ.* **651**, 2228-2234.

Wells, N.S., Baisden, W.T., Horton, T. and Clough, T.J. (2016) Spatial and temporal variations in nitrogen export from a New Zealand pastoral catchment revealed by stream water nitrate isotopic composition. *Water Resour. Res.* **52**, 2480-2854.

Wells, N.S. and Eyre, B.D. (2019) $\delta^{15}N$ patterns in three sub-tropical estuaries show switch from nitrogen 'reactors' to 'pipes' as degradation increases. *Limnol. Oceanograph.* **64**, 860-876.

Wells, N.S., Maher, D.T., Huang, P., Erler, D.V., Maxwell, P., Hipsey, M.R. and Eyre, B.D. (2020) Land-use intensity alters both the source and fate of CO_2 within eight sub-tropical estuaries. *Geochim Cosmochim Ac* **268**, 107-122.

Wickham, H. (2016) ggplot2: Elegant Graphics for Data Analysis. Springer-Verlag New York, https://ggplot2.tidyverse.org.

Wollheim, W.M., Bernal, S., Burns, D.A., Czuba, J.A., Driscoll, C.T., Hansen, A.T., Hensley, R.T., Hosen, J.D., Inamdar, S., Kaushal, S.S., Koenig, L.E., Lu, Y.H., Marzadri, A., Raymond, P.A., Scott, D., Stewart, R.J., Vidon, P.G. and Wohl, E. (2018) River network saturation

concept: factors influencing the balance of biogeochemical supply and demand of river networks. *Biogeochem.* **141**, 503-521.
Wu, S., Chen, J., Li, C., Kong, D.L., Yu, K., Liu, S.W. and Zou, J.W. (2018) Diel and seasonal nitrous oxide fluxes determined by floating chamber and gas transfer equation methods in agricultural irrigation watersheds in southeast China. *Environ. Monit. Assess.* **190**, 14.
Xia, X.H., Liu, T., Yang, Z.F., Michalski, G., Liu, S.D., Jia, Z.M. and Zhang, S. (2017) Enhanced nitrogen loss from rivers through coupled nitrification-denitrification caused by suspended sediment. *Sci. Total Environ.* **579**, 47-59.
Xu, M.N., Li, X.L., Shi, D.L., Zhang, Y., Dai, M.H., Huang, T., Glibert, P.M. and Kao, S.J. (2019) Coupled effect of substrate and light on assimilation and oxidation of regenerated nitrogen in the euphotic ocean. *Limnol. Oceanograph.* **64**, 1270-1283.
Yang, X.Q., Jomaa, S., Buttner, O. and Rode, M. (2019) Autotrophic nitrate uptake in river networks: A modeling approach using continuous high-frequency data. *Water Res* **157**, 258-268.
Yoshida, N. and Toyoda, S. (2000) Constraining the atmospheric N_2O budget from intramolecular site preference in N_2O isotopomers. *Nature* **405**, 330-334.
Zarnetske, J.P., Haggerty, R., Wondzell, S.M., Bokil, V.A. and Gonzalez-Pinzon, R. (2012) Coupled transport and reaction kinetics control the nitrate source-sink function of hyporheic zones. *Water Resour. Res.* **48**, 15.

Supplemental Material

for

Flow regulates biological NO_3^- and N_2O production in a turbid sub-tropical stream

by

Naomi S. Wells & Bradley D. Eyre

submitted to

Geochimica et Cosmochimica Acta

1. Gas transfer velocity

We calculated the gas transfer velocity of N_2O (k_{600}, in m d^{-1}) between the surface water and the air using three empirical parameterisations from (Raymond et al., 2012):

(1) $$k_{600} = (v \times S)^{0.89} \times h^{0.54} \times 5037$$

(2) $$k_{600} = 929 \times (v \times S)^{0.75} \times Q^{0.011}$$

(3) $$k_{600} = 4725 \times (v \times S)^{0.86} \times Q^{-0.14} \times h^{0.66}$$

where v is the current velocity (m s^{-1}), h is the water depth (m), S is the streambed slope (unitless), and Q is discharge (m^3 s^{-1}). These equations were used to calculate the net flux of N_2O between the air and the water column in .

Table S1 Stream gas transfer velocity (k_{600}) and N_2O flux over five 24 hr periods. Fluxes were calculated as both the arithmetic mean and the sum of values measured every 1 min^{-1} for each 24 hr period, based on the mean of the three k_{600} calculations (outlined above) and the measured dissolved N_2O concentrations relative to air.

Sampling date	k_{600} *m* d^{-1}	**mean N_2O flux** *mg N* m^{-2} d^{1}	**total N_2O flux** *mg N* m^{-2} d^{1}
D1 (11/04/2017)	1.0 ± 0.8	0.58 ± 0.8	0.21
D2 (12/04/2017)	0.66 ± 0.3	0.77 ± 0.5	0.67
D4 (14/04/2017)	1.3 ± 0.3	1.9 ± 0.5	1.6
D6 (16/04/2017)	0.82 ± 0.1	1.6 ± 0.5	1.3
D8 (18/04/2017)	0.73 ± 0.3	1.8 0.9	1.6

2. Stream metabolism calculations

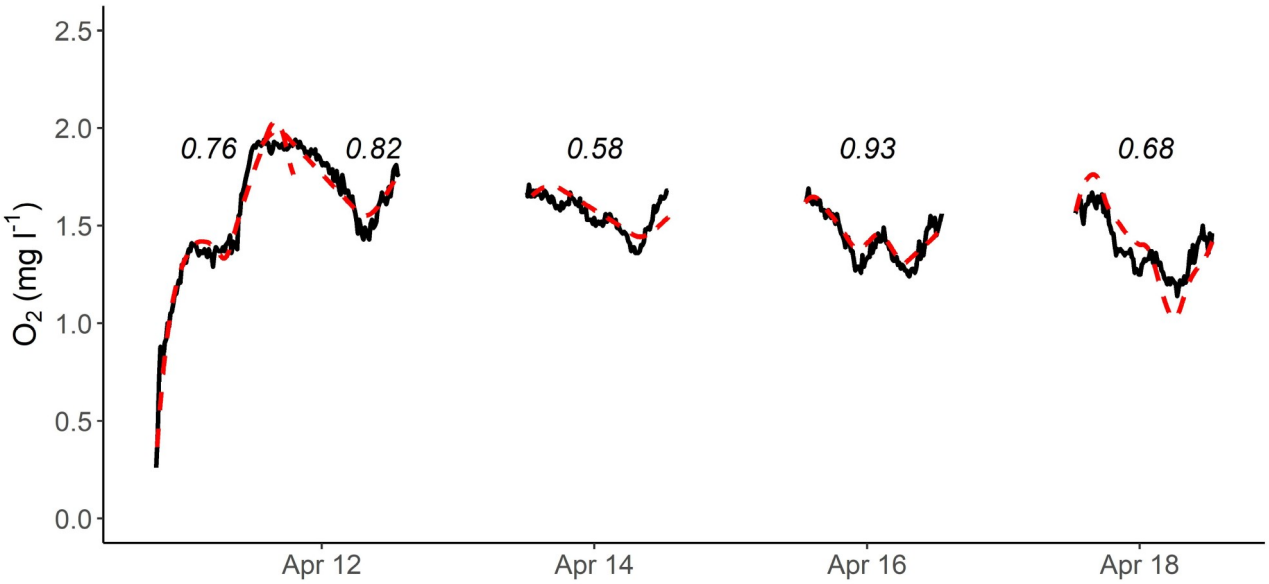

Fig. S1 The measured (black lines) and predicted (red dashed lines) dissolved O_2 concentrations in the surface water at the centre of the sampled reach. Predicted values are based on the best-fit mle solutions in the streamMetabolizer model (Appling et al., 2018). Agreement between measured and modelled values are shown for each 24 h period, based on Kendall correlation analysis.

Table S2 Stream gross primary productivity (GPP) and ecosystem respiration (ER) estimated using the streamMetabolizer R package, using a MLE model for a light saturation effect for GPP and constant ER. Positive fluxes indicate O_2 production, negative fluxes O_2 consumption. The ratio between GPP and ER (P/R) fluxes is also shown.

Sampling date	**GPP** *g O_2 m^{-2} d^{-1}*	**ER** *g O_2 m^{-2} d^{-1}*	**P/R**
D1 (11/04/2017)	2.8	-60 (-65 - -55)	0.05
D2 (12/04/2017)	0.65	-3.3 (-3.3 - -3.3)	0.2
D4 (14/04/2017)	0.32	-2.7 (-2.7 - -2.6)	0.1
D6 (16/04/2017)	0.18	-39 (-38 - -39)	0.005
D8 (18/04/2017)	3.0	-110	0.03

3. Groundwater – surface water mixing calculations

Table S3 The relative contribution of surface water at 20 cm below the streambed surface (f_{sw}) was calculated for each sampled day (D1 – D8) based on the measured conductivity (μS cm^{-1}) in the surface water (*SW*) and hyporheic zone (*HZ*) and range of previously reported local groundwater conductivity (1000 – 5000 μS cm^{-1}).

	D1	D2	D4	D6	D8
Conductivity SW	250	270	300	320	350
Conductivity HZ	680 (50)	610 (100)	650 (80)	990 (100)	1200 (300)
f_{sw} (mean)	0.83	0.86	0.86	0.72	0.62
f_{sw} (high)	0.87	0.92	0.91	0.82	0.82
f_{sw} (low)	0.73	0.75	0.75	0.51	0.24

Table S4 Inputs and outputs from the ^{222}Rn mass balance used to estimate the flux (Q_{GW}) and fraction (f_{GW}) of groundwater in the reach surface water. Losses from radioactive decay (F_{decay}) and water-air evasion (F_{air}) were calculated as dpm reach^{-1}, based on *h* (m) and the stream reach surface area (m^2), using equations from Khadka et al. (2017). Values are reported as mean (min – max) based the minimum and maximum local groundwater ^{222}Rn concentrations for the range of parameters observed over 200 min around daily high (Q_{high}, Rn_{high}) and low (Q_{low}, Rn_{low}) tides.

	D1	D2	D4	D6	D8
F_{decay}	1.5	1.5	1.3	1.4	1.3
F_{air}	57,000	51,000	92,000	76,000	66,000
Q_{low}	0.05 (-0.2 – 0.51)	2.2 (1.9 – 2.6)	5.5 (5.3 – 5.6)	2.0 (1.6 – 2.5)	0.96 (-0.034 – 1.6)
Rn_{low}	4.7 (4.6 – 4.8)	4.1 (4.0 – 4.2)	4.0 (3.9 – 4.0)	4.5 (4.4 – 4.8)	4.1 (4.1 – 4.3)
Q_{high}	3.3 (0.29 – 6.5)	3.3 (3.1 – 3.4)	3.7 (2.5 – 4.7)	2.8 (2.7 – 2.9)	2.3 (1.6 – 3.1)
Rn_{high}	2.9 (1.9 – 3.3)	2.7 (2.1 – 3.2)	3.5 (3.2 – 3.7)	3.8 (3.7 – 3.8)	3.6 (3.6 – 3.7)
Q_{GW}	1.1 (0.25 – 3.0)	1.0 (0.21 – 2.0)	1.9 (0.36 – 3.5)	1.6 (0.33 – 3.2)	1.4 (0.3 – 2.9)
f_{GW}	0.35 ± 0.3	0.32 ± 0.3	0.54 ± 0.4	0.58 ± 0.5	0.61 ± 0.5

4. Additional water chemistry figures and tables

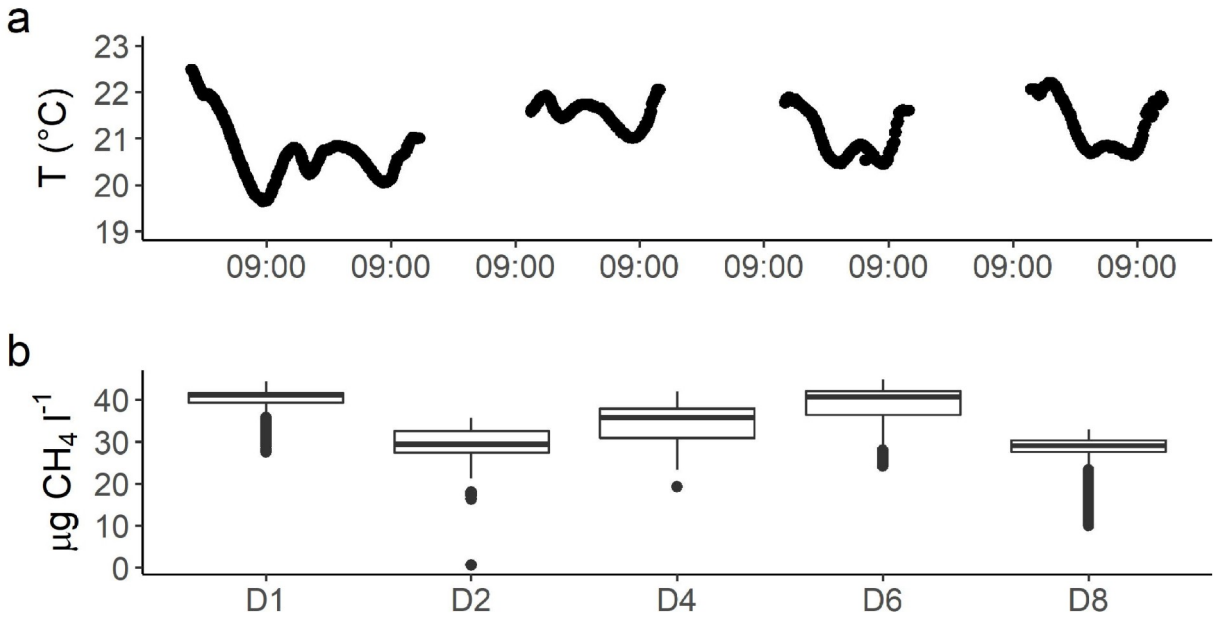

Fig. S2 Changes in surface water temperature (a) and CH_4 (b) over eight days of falling water levels.

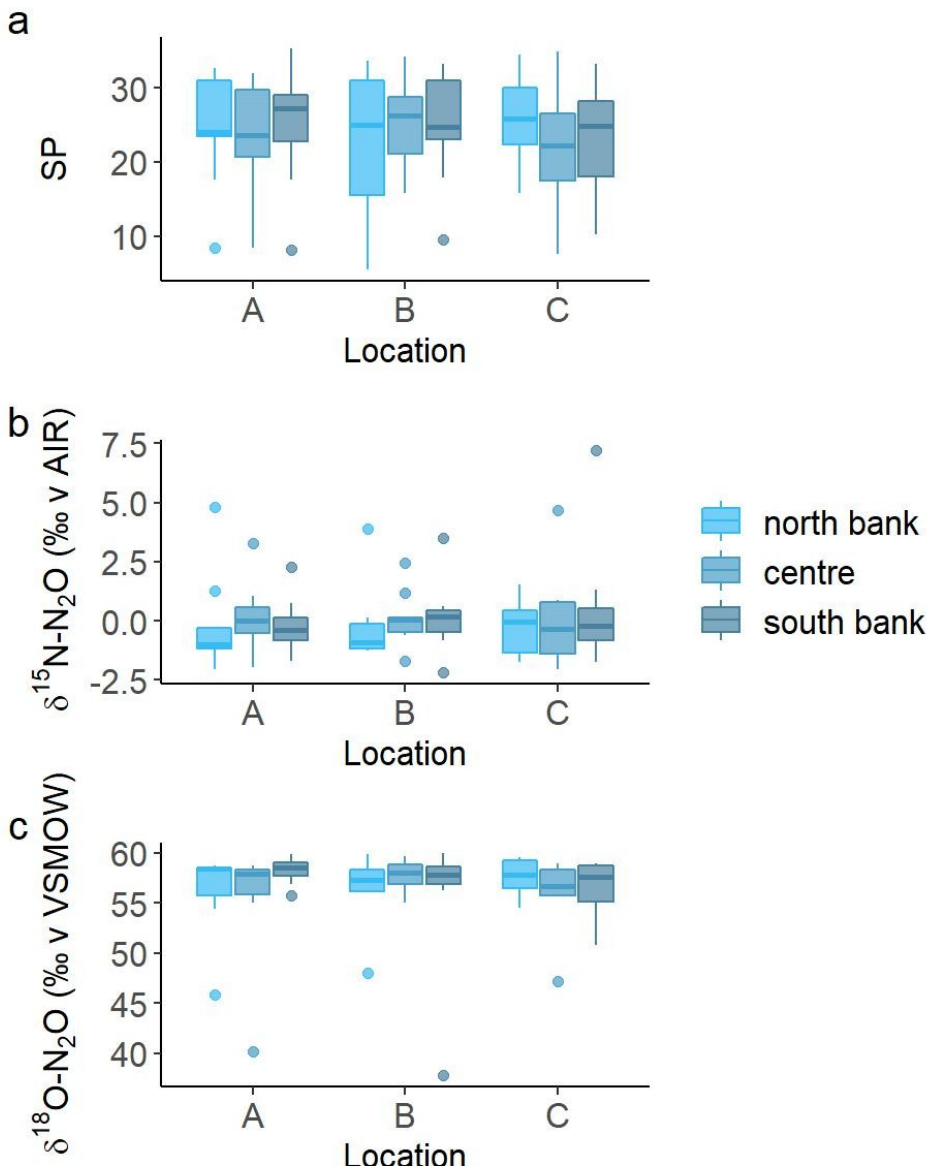

Fig. S3 Differences in the site preference (SP, a), $\delta^{15}N$ (b), and $\delta^{18}O$ (c) composition of surface water N_2O. Boxplots show the mean range of values measured for 10 sampling times over five days. Samples were collected across the width (north bank, centre, and south bank) at three locations along the length of a 50 m stream reach (A, B, C). Values are not corrected for atmospheric mixing.

Table S5 Surface water chemistry, measured at nine locations over the length (A, B, C) and width (north, centre, south) of a stream reach (*SW*). Data shown is the mean (standard deviation) for each sampling location measured 10 times over an eight day period. See Table S8 for statistical tests for the NO_3^- and NH_4^+ data.

Location		NH_4^+ *mg N l^{-1}*	NO_3^- *mg N l^{-1}*	DOC *mg C l^{-1}*	PO_4^{3-} *mg P l^{-1}*
A	North	0.98 (0.8)	1.7 (0.6)	9.4 (2)	0.19 (0.2)
	Centre	0.66 (0.2)	1.7 (0.6)	9.5 (2)	0.18 (0.3)
	South	0.72 (0.03)	1.9 (0.4)	9.5 (1)	0.12 (0.09)
B	North	0.67 (0.07)	1.7 (0.5)	11 (2)	0.10 (0.04)
	Centre	0.69 (0.06)	1.8 (0.5)	9.9 (1)	0.095 (0.01)
	South	0.71 (0.04)	1.9 (0.4)	9.9 (1)	0.091 (0.01)
C	North	0.86 (0.6)	1.8 (0.5)	10 (2)	0.13 (0.1)
	Centre	0.69 (0.05)	1.9 (0.4)	10 (3)	0.094 (0.01)
	South	0.70 (0.04)	1.9 (0.4)	9.9 (1)	0.096 (0.02)

Table S6 Subsurface water chemistry, measured using DET probes inserted to 5 cm below the streambed surface (*S*). Data shown is the mean (standard deviation) for each sampling location measured 10 times over eight days. Note neither DOC nor PO_4^{3-} could be measured in the DET probes.

Location		NH_4^+ *mg N l^{-1}*	NO_3^- *mg N l^{-1}*
A	North	110 (70)	0.32 (0.2)
	Centre	130 (80)	0.23 (0.08)
	South	53 (30)	0.38 (0.2)
B	North	51 (40)	0.42 (0.5)
	Centre	120 (100)	0.51 (0.5)
	South	61 (70)	0.53 (0.3)
C	North	42 (20)	0.31 (0.2)
	Centre	110 (50)	0.38 (0.2)
	South	79 (30)	0.82 (0.5)

Table S7 Subsurface water chemistry, measured in peizometers at 20 cm below the streambed surface (*HZ*). Data shown is the mean (standard deviation) for each sampling location measured 10 times over an eight day period; see Table S8 for statistical analyses of spatial and temporal patterns.

Location		NH_4^+ *mg N l^{-1}*	NO_3^- *mg N l^{-1}*	DOC *mg C l^{-1}*	PO_4^{3-} *mg P l^{-1}*
A	North	4.7 (0.9)	0.047 (0.03)	92 (60)	0.066 (0.05)
	Centre	1.1 (0.8)	0.27 (0.2)	53 (20)	0.073 (0.04)
	South	1.0 (0.3)	1.1 (0.4)	51 (20)	0.21 (0.1)
B	North	1.5 (0.7)	0.17 (0.2)	60 (30)	0.37 (0.2)
	Centre	0.78 (0.08)	1.6 (0.4)	27 (5)	0.099 (0.03)
	South	0.73 (0.05)	1.8 (0.4)	20 (4)	0.097 (0.03)
C	North	0.74 (0.4)	0.14 (0.2)	70 (30)	0.23 (0.2)
	Centre	0.75 (0.07)	1.7 (0.5)	23 (9)	0.17 (0.2)
	South	1.3 (0.6)	1.5 (0.4)	27 (20)	0.26 (0.05)

Table S8 Mixed model results (as Type II Wald F tests and 95% confidence intervals) for changes in NO_3^- concentrations, $\delta^{15}N\text{-}NO_3^-$, and $\delta^{18}O\text{-}NO_3^-$ over time. Sampling locations are treated as repeated measures within each (*SW*, *S*, *HZ*), which were evaluated separately. Specific sample locations are treated as random effects, and time (continuous) and locations, either width-wise (north, centre, south) and length-wise (A, B, C), as fixed factors. **Bold** text indicates significant differences (* = $p<0.05$, ** = $p<0.01$, *** = $p<0.001$).

Depth	Parameter	Time		Width		Time*Width		Length		Time*Length	
SW	NO_3^-	**410*** **	**(7 – 9)**	4.6	(-80 – 400)	1.3	(-3 – 1)	0.60	(-70 – 300)	0.40	(-3 – 1)
	NH_4^+	3.3	(-5 - -1)	1.7	(-700 - -90)	**3.5***	**(0.3 – 6)**	0.54	(-500 – 300)	0.86	(-3 – 5)
	$\delta^{18}O\text{-}NO_3^-$	**24*** **	**(-0.05 - -0.1)**	0.18	(-3 – 2)	0.39	(-0.01 – 0.03)	0.48	(-2 – 3)	0.77	(-0.03 – 0.02)
	$\delta^{15}N\text{-}NO_3^-$	**93*** **	**(0.008, 0.02)**	0.75	(-0.08 – 0.9)	0.79	(-0.006 – 0.004)	1.9	(-1 – 0.3)	0.62	(-0.005 – 0.005)
S	NO_3^-	1.9	(-2 – 2)	2.2	(-200 – 700)	0.83	(-5 – 2)	1.2	(-10 – 600)	0.78	(-5 – 3)
	NH_4^+	3.3	(-5 - -1)	1.7	(-700 - -90)	**3.5***	**(0.3 – 7)**	0.54	(-500 – 300)	0.86	(-3 – 5)
	$\delta^{18}O\text{-}NO_3^-$	0.43	(-0.02 – 0.03)	0.91	(-6 – 6)	**2.8***	**(-0.08 – -0.004)**	0.32	(-8 – 3)	0.82	(-0.02 – 0.06)
	$\delta^{15}N\text{-}NO_3^-$	**9.6** **	**(-0.02 – 0.04)**	1.1	(-8 – 6)	2.3	(-0.03 – 0.1)	0.47	(-4 – 8)	0.71	(-0.08 – 0.02)
HZ	NO_3^-	**17*** **	**(-3 – 0.2)**	**5.8***	**(200 – 1000)**	**12*** **	**(3 – 8)**	0.78	(-800 – 2000)	**4.98** **	**(1 – 6)**
	NH_4^+	**24*** **	**(4 – 10)**	1.3	(-3000 – 800)	2.6	(-8 – 0.1)	1.0	(-3000 – 800)	1.8	(-8 – 0.7)
	$\delta^{18}O\text{-}NO_3^-$	1.1	(-0.005 – 0.06)	**5.4***	**(-8 – 3)**	1.6	(-0.08 – 0.03)	0.31	(-7 – 5)	0.11	(-0.05 – 0.04)
	$\delta^{15}N\text{-}NO_3^-$	0.33	(-0.07 – -0.02)	4.5	(-11 – -3)	**5.0** **	**(0.02 – 0.1)**	1.0	(-10 – 0.8)	1.9	(-0.02 – 0.08)

References

Appling, A.P., Hall Jr., R.O., Yackulic, C.B. and Arroita, M. (2018) Overcoming equifinality: Leveraging long time series for stream metabolism estimation. *J. Geophys. Res- Biogeosci.* **123**, 624-645.

Khadka, M.B., Martin, J.B. and Kurz, M.J. (2017) Synoptic estimates of diffuse groundwater seepage to a spring-fed karst river at high spatial resolution using an automated radon measurement technique. *J. Hydrol.* **544**, 86-96.

Raymond, P.A., Zappa, C.J., Butman, D., Bott, T.L., Potter, J., Mulholland, P., Laursen, A.E., McDowell, W.H. and Newbold, D. (2012) Scaling the gas transfer velocity and hydraulic geometry in streams and small rivers. *Limnology & Oceanography: Fluids and Environments* **2**, 41-53.